Anonymous Referee #1

The authors present a simultaneous field measurement dataset of BC at five sites in this paper with the aim to investigate the intra-regional transport between the south edge of North China Plain and Central China based on the variations of BC mass concentration, sources and optical properties. The dataset is important and would be with good scientific significance to help people to model the BC aerosol climate effect in East Asian by studying the changes of BC physio-chemical and optical properties during the transport. My major concern is, as the authors stated in their paper (in the introduction), one of the key purpose of this study were to quantify the regional transportation of BC at multiple observation sites in CC and SE-NCP. But the backward trajectory method used by the authors can just get some qualitative analysis of the air parcels transport as presented in their study. The paper will be greatly improved if the authors consider using models to simulate the emissions and then to quantify the intra-regional contributions at the sites based on the measured BC concentration data. In addition, there are also a lot of language issues and editing needs that have to be addressed. The authors thus need to make a careful revision and correction on the language, especially revisions on some seemingly illogical expression, to improve the overall quality of the paper for publication in the journal. I would recommend the editor to reconsider the papers after a major revision by the authors.

AR: Thanks for your comment. We have added the Geos-Chem simulation to quantify the transport contributions. However, the Geos-Chem results are not good enough and details are provided in the response to Comment 10. Additionally, we have also carefully checked and polished the language.

Other specific comments,

1. Section 3.1, the authors should more focus on discussing and comparing the different BC levels between the studied 5 sites and other regions in China or over the globe, not on North China and other regions.

AR: Thanks for your suggestion and we do the literatures review. Comparison of BC in this study and other regions was listed in the supplementary file Fig. R1:

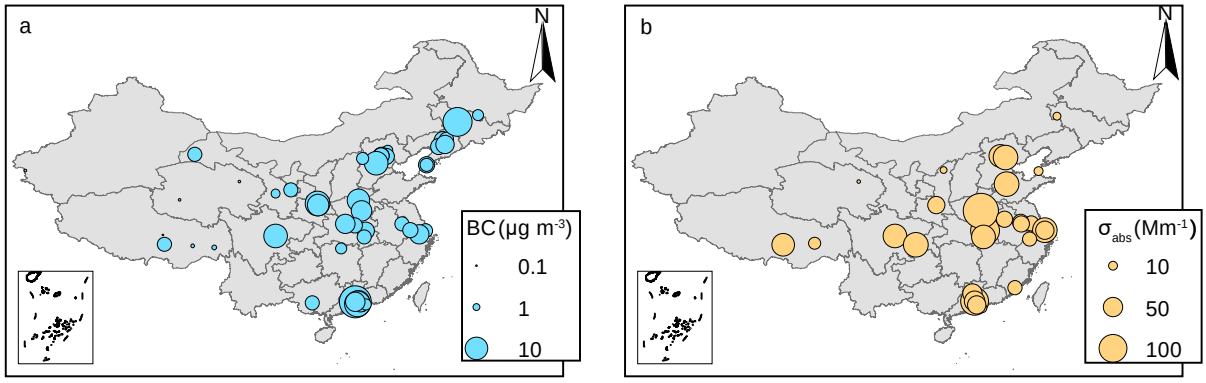

Figure. R1 Spatial distribution of BC mass concentration (a) and absorption coefficients (b) in China. More details can be found in Table S1 and S2 in the supplementary materials.

As Table S1 shown, BC was generally higher in North China and lower BC levels were found in remote areas and coastal areas as Fig. 3a shows. Wang et al, (2014b) analyzed ambient BC in an urban site in Xi'an during winter and found the average mass concentration was 8.8 ± 3.7 μg m^{-3}, which was higher than that in this study. Compared to other regions, BC levels in this study were higher than a remote area of Lulang in southeastern part of the Tibetan Plateau (0.31

± 0.55 μg m^{-3}) (Wang et al., 2018) as well as coastal areas such as Hong Kong (1.4 ± 1.1 μg m^{-3}) (Wang et al., 2017a) and a rural site in Shenzhen (2.6 ± 1.0 μg m^{-3}) (Huang et al., 2012).

References

Huang, X.F., Sun, T.L., Zeng, L.W., Yu, G.H. and Luan, S.J.: Black carbon aerosol characterization in a coastal city in South China using a single particle soot photometer, Atmos. Environ., 51, 21–28, doi:10.1016/j.atmosenv.2012.01.056, 2012.

Wang, Q., Huang, R.J., Cao, J., Han, Y., Wang, G., Li, G., Wang, Y., Dai, W., Zhang, R. and Zhou, Y.: Mixing state of black carbon aerosol in a heavily Polluted urban area of China: Implications for light Absorption enhancement, Aerosol Sci. Technol., 48(7), 689–697, doi:10.1080/02786826.2014.917758, 2014b.

Wang, J., Virkkula, A., Gao, Y., Lee, S., Shen, Y., Chi, X., Nie, W., Liu, Q., Xu, Z., Huang, X., Wang, T., Cui, L. and Ding, A.: Observations of aerosol optical properties at a coastal site in Hong Kong, South China, Atmos. Chem. Phys., 17(4), 2653–2671, doi:10.5194/acp-17-2653-2017, 2017a.

Wang, Q., Cao, J., Han, Y., Tian, J., Zhu, C., Zhang, Y., Zhang, N., Shen, Z., Ni, H., Zhao, S. and Wu, J.: Sources and physicochemical characteristics of black carbon aerosol from the southeastern Tibetan Plateau: internal mixing enhances light absorption, Atmos. Chem. Phys., 18(7), 4639–4656, doi:10.5194/acp-18-4639-2018, 2018.

2. Line 214, ". . .Despite the sampling periods, site types, inlet of aerosol and instruments were different between different studies (Table S1), BC was generally higher in North China and lower BC levels were found in remote areas and coastal areas... " Here, it is not appropriate and logical expression by saying the two things using the "despite".

AR: We have corrected it as above.

3. Line 242 "..At WH, the concentration and percentage of BC_{bb} both decreased from clean to pollution, which suggested that more BCff was emitted during haze episodes...", should revise as "... both the concentration and percentage of BC_{bb} decreased from clean to pollution". . ." also, you say more fossil fuel BC was emitted. But the increased BC is probably due to the accumulation of pollutes during polluted days when the PBL is lowered.

AR: Thanks for your correction, and we have revised it.

4. Lines 248-250, ". . .the pollution episodes (Huang et al., 249 2014), and the increased secondary aerosols would be more adsorbed on the surface of BC. . .." Do you mean that more secondary aerosols will be coated on BC? "...the σabs also elevated by 11.7−254% as the air quality switched from clean to pollution (Fig. 4e). There are more secondary aerosols (i.e., sulfate, nitrate) during the pollution episodes (Huang et al., 249 2014),.." Do you have some observations of chemical composition that would support your conclusions.

AR: Yes, we have conducted the off-line low volume $PM_{1.0}$ sampling and chemical analysis at the five sites during the field sampling campaign. Here, we just show part of the chemical analysis results (which have not been published) to support that there were more sulfate and nitrate during the pollution episodes as shown in the following figure.

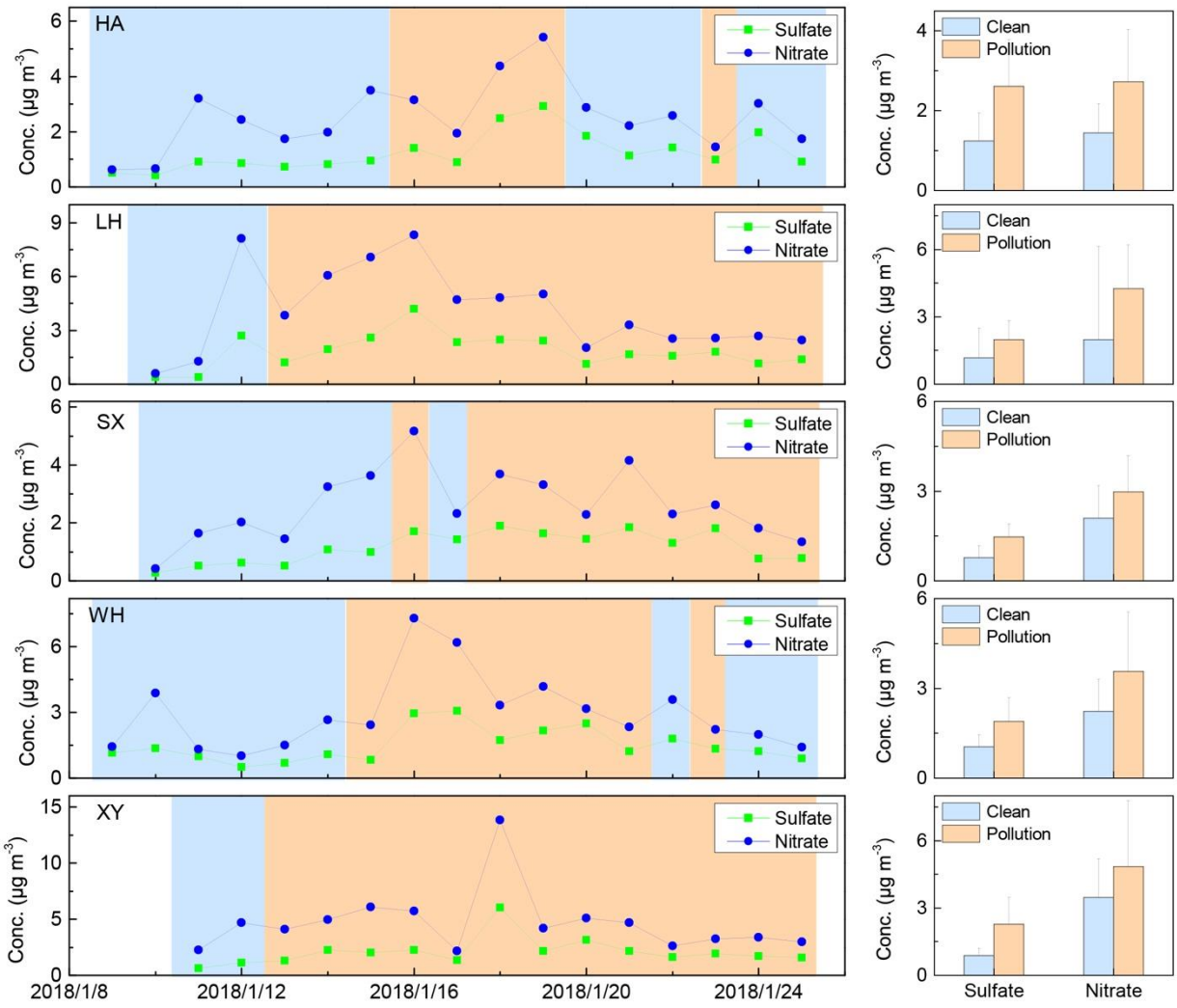

Fig. R2 Daily concentrations of sulfate (green line) and nitrate (blue line) during observation (left panel) and their average concentrations for clean days (blue) and pollution episodes (orange) (right panel).

5. Line 253, "The decreasing of AAE from clean to polluted days was also reported else- where (Zhang et al., 2015b) and it can be partly attributed to the source variation. . .", the AAE is very sensitive to particles size, so you may need to think about the particles growth due to the secondary formation processes.

AR: Thanks for your comments and we agree with you. However, we did mot measure the particle size during our observation, and we try our best to explain the decreasing of AAE during pollution episodes according to previous studies and the sentences are revised as following:

The AAE is also sensitive to other factors such as the particle size. Previous studies suggested that the particle diameter and number concentration increased from clean to pollution episodes due to several factors such as coagulation, hygroscopic growth, emissions, meteorological conditions, i.e., planetary boundary layer and wind speed (Guo et al., 2014; Zhang et al., 2017). These studies suggested that the particle diameter is generally larger during pollution days. Furthermore, the lab combustion and numeric simulation proved that BC particle with larger geometric median diameter had lower AAE value (Singh et al., 2016; Liu et al., 2018b). Therefore, lower AAE was observed during pollution episodes in this study.

References

Guo, S., Hu, M., Zamora, M. L., Peng, J., Shang, D., Zheng, J., Du, Z., Wu, Z., Shao, M., Zeng, L., Molina, M. J. and Zhang, R.: Elucidating severe urban haze formation in China, Proceedings of the National Academy of Sciences, 111(49), 17373–17378, doi:10.1073/pnas.1419604111, 2014.

Liu, C., Chung, C. E., Yin, Y. and Schnaiter, M.: The absorption Ångström exponent of black carbon: from numerical aspects, Atmospheric Chemistry and Physics, 18(9), 6259–6273, doi:10.5194/acp-18-6259-2018, 2018.

Singh, S., Fiddler, M. N. and Bililign, S.: Measurement of size-dependent single scattering albedo of fresh biomass burning aerosols using the extinction-minus-scattering technique with a combination of cavity ring-down spectroscopy and nephelometry, Atmospheric Chemistry and Physics, 16(21), 13491–13507, doi:10.5194/acp-16-13491-2016, 2016.

Zhang, K., Wang, D., Bian, Q., Duan, Y., Zhao, M., Fei, D., Xiu, G. and Fu, Q.: Tethered balloon-based particle number concentration, and size distribution vertical profiles within the lower troposphere of Shanghai, Atmospheric Environment, 154, 141–150, doi:10.1016/j.atmosenv.2017.01.025, 2017.

6. Lines 257-267, you only show the diurnal variations of mass concentrations of BC, how about the absorption coefficient?

AR: Thanks for your suggestion, and we found that the diurnal variations of absorption coefficient and BC levels were similar as the following figure shown.

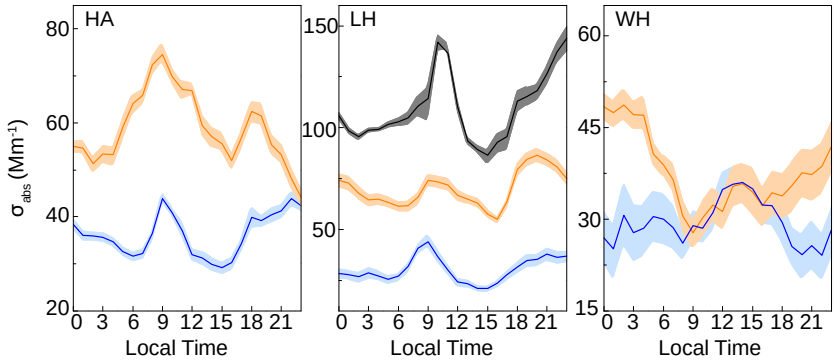

Fig. R3 Diurnal variations of BC absorption coefficients. (The figure has been added as Fig. S7 in the supplementary materials of the revised version)

In the revised manuscript, we have revised this part as following:

Figure 6 and Fig. S7 shows the diurnal variations of eBC and absorption coefficients under different air quality. The diurnal cycles of black carbon and absorption showed similar variation patterns. The BC mass concentrations were discussed here.

7. Line 271, You say ". . .combustion (traffic) and agricultural burning are higher than those from industrial emissions such as manufacturing and mineral products. But you give an example for the lower ratios from residential wood combustion, which is not an industrial source.

AR: Thanks for your comment. We have carefully checked the reference (Chow et al., 2011). The ratios of BC/$PM_{2.5}$ from mobile sources and area sources were generally higher than that from industrial sources and we have revised this part as following:

Generally, the ratios of BC/$PM_{2.5}$ from mobile sources (0.059-0.74) and area sources (0.032-0.33) were higher than that from industrial sources (0.0046-0.03). For instance, the mobile sources hold the highest ratios of BC/$PM_{2.5}$ (0.33−0.77) and the cement kiln showed lower ratio (0.03) (Chow et al., 2011).

References

Chow, J. C., Watson, J. G., Lowenthal, D. H., Antony Chen, L.-W. and Motallebi, N.: $PM_{2.5}$ source profiles for black and organic carbon emission inventories, Atmos. Environ.,, 45(31), 5407–5414, doi:10.1016/j.atmosenv.2011.07.011, 2011.

8. L291, It would be more interesting if you discuss whether the BC at downwind sites is more aged because of the transportation, because you say that ". . .the BC/CO is used to reflect the BC aging during the transport.

AR: We feel sorry that we did not discuss the aging of BC during the transport by BC/CO ratio. We have tried to discuss the BC/CO ratio using the same method in section 3.6, however, the low data resolution of CO (1-hour) would cause large uncertainty. So, we used the AAE instead of BC/CO ratio to discuss the BC aging during the transportation from upwind to downwind site. The decreasing of AAE from upwind to downwind site suggested that the BC was aged during the transportation and more details can be found in section 3.6.

9. Line 307, ". . ...The same result was also found at WH. High level of BCbb was due to more biomass burning in the southeast direction of HA and WH. . ."How do you know that more biomass burning in the southeast? Do you have some evidences to support your statement?

AR: We draw this conclusion because there were more fire spots in the southeast direction of WH during the study period as shown in Fig. R4. We have revised this part.

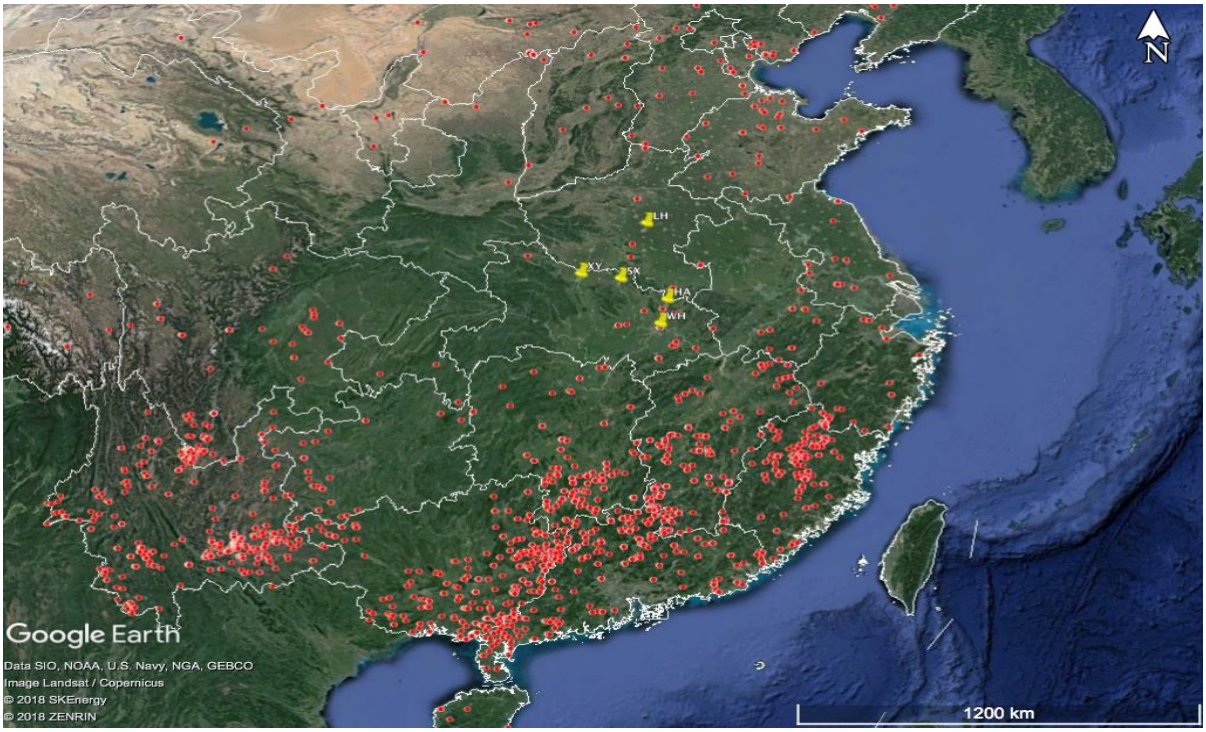

Figure R4 Locations of the fire spots downloaded from MODIS during the observation period (2018/1/08~2018/1/25).

10. Section 3.5, The paragraph may need to revise very carefully for that the current statements on the influences of the air parcels (CWT analysis) on each site are too trivial and wordy to understand. The authors are suggested to simulate the emissions and to quantify the intra-regional contributions at the sites based on the measured BC concentration data by using regional models.

AR: Thanks for your suggestion, we have tried Geos-Chem model to simulate the intra-regional transport contribution. The settings of Geos-Chem are described as the following part:

We use the nested GEOS-Chem model for China (version 11-01, http://wiki.seas.harvard.edu/geos-chem/index.php/Main_Page) to simulate the surface BC concentration. Driven by the GEOS-FP assimilation meteorology from the Goddard Earth Observing System (GEOS) of the NASA Global Modeling and Assimilation Office, the nested model has a horizontal resolution of 0.3125° longitude × 0.25° latitude with 47 vertical layers, and the lowest 10 layers are of ~130 m thickness each. The lateral boundary conditions of nested model are taken every 3 hours from a global GEOS-Chem simulation at 2.5° long × 2° lat horizontally. Spin-up time for nested model and global model are 15 days and one month, respectively. The scheme of planetary boundary layer employs a non-local scheme following Lin et al. (2010). Model convection is simulated with the relaxed Arakawa–Schubert scheme (Rienecker et al., 2008). Both the global and nested GEOS-Chem models are run with the NO_x-O*x*-hydrocarbon-aerosol-bromine tropospheric chemistry mechanism with online aerosols. Aerosols simulated by model include secondary inorganic aerosols (SIOA, including sulfate, nitrate and ammonium), secondary organic aerosols (SOA), primary organic aerosols (POA), black carbon (BC), dust and sea salts.

Monthly gridded anthropogenic emissions in China are taken from the Multi-resolution Emission Inventory for China (MEIC, www.meicmodel.org; Geng et al., 2017) of 2016 for nitrogen oxides (NO_x), carbon monoxide (CO), sulfur dioxide (SO_2), BC and POA. Following Zhang et al. (2015), emissions of anthropogenic fine dust are also included as primary $PM_{2.5}$ excluding BC and POA from MEIC in 2012. Biomass burning emissions are taken from the monthly GFED4 datasets (Giglio et al., 2013). Biogenic emissions of NMVOC follow MEGANv2.1 (Guenther et al., 2012). Soil emissions of NO_x employ the parameterization from Hudman et al. (2012).

Control and two sensitivity simulations were also done to study the regional transport contribution. The settings of control simulation were described above, and the sensitivity simulation were done with the emissions from Hubei and Henan province being closed, respectively.

The simulated and observed time series of BC at the five sites are shown in the Fig. R5. The Pearson coefficients (*r*) and NMB ranged from -0.44 to 0.07 and -39.9 to 19.8%, respectively, which suggested that the Geos-Chem is not good enough to reconstruct the BC variation in this study. There are several reasons: (1) the emission inventory uncertainty due to activity data, emission factors for energy-related combustion; burned area, fuel load and combustion completeness and emission factor for open burning emissions (Bond et al., 2013); low temporal resolution (i.e., monthly in this study); (2) the uncertainty of the input reanalysis meteorological field (i.e., in this study); (3) simple physical-chemical mechanism of BC in code, etc. More accurate and quantitative modeling for regional transportation of BC should be done after the above problems improved in the future.

Considering the poor simulation result, the Geos-Chem results were not adopted in the revised manuscript. Additionally, we carefully revised section 3.5 as the following:

Employing CWT method, the potential geographic origins of eBC for the five sites were explored (Fig. S11). Overall, CWT results of eBC at the five sites suggested that high eBC levels were found both in the north and south directions of LH and WH, while the high levels (i.e., > 4 μg m^{-3}) of eBC were only found from northeast directions of HA, SX and XY (Fig. S11). Additionally, the potential geographic source regions of BC_{bb} and BC_{ff} at HA, LH and WH were also discussed as shown in Fig. 10. At HA, the CWT results showed that high levels of eBC (i.e., > 3 μg m^{-3}) were from north/northeast direction. However, the hot spots of BC_{bb} and BC_{ff} were different, with higher levels of BC_{bb} from both south and north

directions and higher levels of BC_{ff} from the north direction. Also, higher levels of BC_{bb} and BC_{ff} were found in the south of LH. Opposite to the CWT results at HA, the hot spots of BC_{bb} was only found in the southeast direction of WH and high levels of BC_{ff} were found in the north and south directions of WH. The CWT results at WH were in line with the CBPF plots in section 3.4. The unity of CWT and CBPF results at WH suggested that there were intensive biomass burning activities in the south direction of WH during the observation period, which was verified by the MODIS fire-points distribution (Fig. S10).

We also discussed the source region differences of BC under different air quality (Fig. 11). The higher levels (>1 μg m^{-3}) of eBC, BC_{bb} and BC_{ff} were mainly from the south direction of three sites when the air was clean, while during the pollution episodes, air parcels from the north direction contributed high concentrations. For instance, at WH, high levels of eBC (> 2.5 μg m^{-3}) were found from south direction, while the source regions with high level eBC (> 3 μg m^{-3}) switched to northeast direction when the air quality was worsened. Figure 12 shows the semiquantitative results of transportation contribution results during clean and pollution episodes. At the boundary sites (HA, SX and XY), BC was mainly from south direction (accounting for 46.0−58.2%) when the air quality was clean, and it was mainly from northeast/northwest directions (51.2−76.5%) when the air quality getting worse. At SE-NCP site (LH), BC was dominantly from south direction (47.8%) during pollution episodes. At CC site (WH), BC was mainly from northeast direction (49.3−71.1%). These results suggested that northwest and northeast directions were the main transport pathways of air pollutants reaching to WH during the pollution episodes. Furthermore, to control local emissions during haze episodes, the emission sources, i.e., industry plant and open biomass burning in the upwind direction should also be controlled to prevent the further deterioration of air quality in downwind areas.

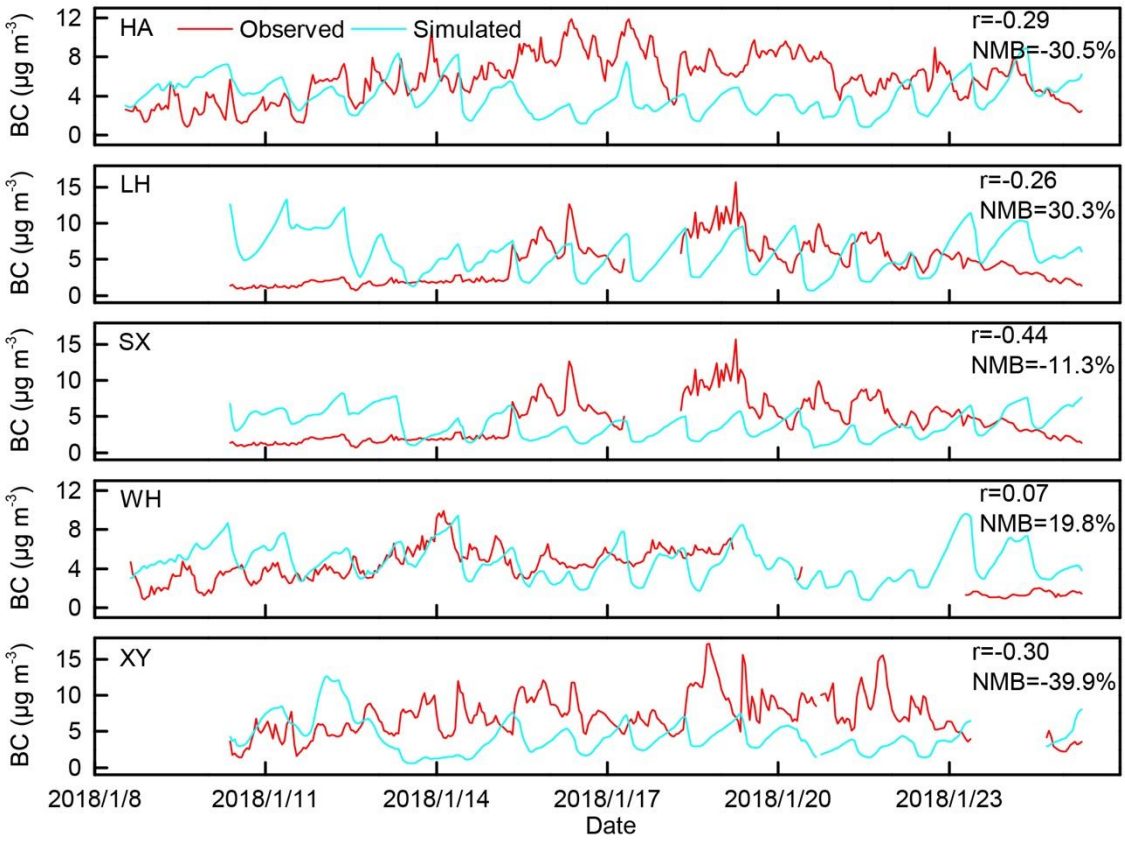

Figure. R5 Time series of observed and simulated BC concentrations from Goes-Chem model during the study period.

References

Bond, T. C., Doherty, S. J., Fahey, D. W., Forster, P. M., Berntsen, T., DeAngelo, B. J., Flanner, M. G., Ghan, S., Kärcher,

B., Koch, D., Kinne, S., Kondo, Y., Quinn, P. K., Sarofim, M. C., Schultz, M. G., Schulz, M., Venkataraman, C., Zhang, H., Zhang, S., Bellouin, N., Guttikunda, S. K., Hopke, P. K., Jacobson, M. Z., Kaiser, J. W., Klimont, Z., Lohmann, U., Schwarz, J. P., Shindell, D., Storelvmo, T., Warren, S. G. and Zender, C. S.: Bounding the role of black carbon in the climate system: A scientific assessment, J. Geophys. Res, Atmos., 118(11), 5380–5552.

Geng, G., Zhang, Q., Martin, R. V., Lin, J.-T., Huo, H., Zheng, B., Wang, S., and He, K., 2017. Impact of spatial proxies on the representation of bottom-up emission inventories: A satellite-based analysis. Atmos. Chem. and Phys., 17, 4131-4145.

Giglio, L., J. T. Randerson, and G. R. van der Werf, 2013. Analysis of daily, monthly, and annual burned area using the fourth-generation global fire emissions database (GFED4)", J. Geophys. Res, Biogeosciences. 118, Issue 1, 317-328. Guenther, A. B., Jiang, X., Heald, C. L., Sakulyanontvittaya, T., Duhl, T., Emmons, L. K., and Wang, X., 2012. The Model of Emissions of Gases and Aerosols from Nature version 2.1 (MEGAN2.1): an extended and updated framework for modeling biogenic emissions. Geosci. Model Dev., 5, 1471-1492.

Hudman, R.C., N.E. Moore, R.V. Martin, A.R. Russell, A.K. Mebust, L.C. Valin, and R.C. Cohen, 2012. A mechanistic model of global soil nitric oxide emissions: implementation and space based-constraints. Atmos. Chem. Phys., 12, 7779-7795.

Lin, J., McElroy, M.B., 2010. Impacts of boundary layer mixing on pollutant vertical profiles in the lower troposphere: Implications to satellite remote sensing. Atmos. Environ., 44, 1726-1739.

Rienecker, M. M., Suarez, M. J., Todling, R., Bacmeister, J., Takacs, L., Liu, H.-C., Gu, W., Sienkiewicz, M., Koster, R. D., Gelaro, R., Stajner, I., and Nielsen, J. E.: The GEOS-5 Data Assimilation System – Documentation of Versions 5.0.1, 5.1.0, and 5.2.0, Technical Report Series on Global Modeling and Data Assimilation, NASA Tech. Memo. NASA TM/2008-104606, Vol. 27, 118 pp., 2008.

Zhang L., Liu, L., Zhao, Y.H., Gong, S.L., Zhang, X.Y., D. K. Henze, S. L. Capps, Tzung-May Fu, Zhang, Q., Wang, Y.X., 2015. Source attribution of particulate matter pollution over North China with the adjoint method. Environ Res Lett. 10, 084011.

11. Line 367, ". . .the travelling time (aging time) from LH to HA and from HA to LH were 28 h and 31 h, respectively, which suggested that the BC particle should be coagulated through complex atmospheric processes. Therefore, the new emission inputs along the trajectory enhanced the eBC mass concentration during the transport. . .." How do you infer that "the new emission" enhanced the eBC mass concentration from the previous sentence (longer aging time and coagulation processes) here?

AR: We have revised this part as the following:

Atmospheric removal of BC occurs in a few days to weeks via wet and dry depositions or contact with surfaces (Bond et al., 2013). In these two cases, there were no precipitation events and the transport time was short (i.e., 28 and 31h), which suggested the less removal rates. Therefore, the new emission inputs along the trajectory enhanced the eBC mass concentration during the transport

Previous study found that the BC coagulation with non-refractory materials becomes more significant when the aging timescale was greater than 10 h (Riemer et al., 2004). Chamber studies and field observations also found that the BC absorption enhancement under polluted urban ambient air (Peng et al., 2016, Zhang et al., 2018, Wang et al., 2018c), suggesting the role of aging in modifying BC optical properties. In these two cases, the travelling time (aging time) from LH to HA and from HA to LH was 28 h and 31 h, respectively, which suggested that the BC particle should be coagulated through complex atmospheric processes. Therefore, the σ_{abs} *was found increased from upwind to downwind site. On the contrary, the AAE values were found decreased during the transport. The AAE is sensitive to the particle size. A lab*

combustion experiment showed that the particles with smaller diameter from fresh biomass burning have lower AAE value than larger particles (Singh et al., 2016). Simulation also confirmed that the AAE of BC particle decreased with the increasing of its geometric median diameter (Liu et al., 2018b). Therefore, the diameter of BC particle increased during the transportation due to the aging processes supported by the increased absorb coefficients and decreased AAE as discussed above.

12. Line 370, "...However, slight differences found for BCbb transport: BCbb increased from LH (1.28 ± 0.06 μg m−3) to HA (2.57 ± 0.47 μg m−3), while BCbb decreased from HA (2.37 ± 0.23 μg m−3) to LH (2.14 ± 0.14 μg m−3). . ." What do you mean about this?

AR: In this sentence, we want to express the BC emission difference in these two regions. In case 1, air masses transported from LH (Henan province in north direction) to HA (Hubei province in south direction), both the eBC and BC_{bb} increased However, in Case 2, air masses transported from HA to LH, despite the eBC increased, the BC_{bb} decreased due to less BC emissions in Hubei province than those in Henan province. BC emission inventories also showed this difference (Qin and Xie, 2009, Qiu et al., 2016).

References

Qin, Y. and Xie, S. D.: Spatial and temporal variation of anthropogenic black carbon emissions in China for the period 1980–2009, Atmos. Chem. Phys., 12(11), 4825–4841, doi:10.5194/acp-12-4825-2012, 2012.

Qiu, X., Duan, L., Chai, F., Wang, S., Yu, Q. and Wang, S.: Deriving high-resolution emission inventory of open biomass burning in China based on satellite observations, Environ. Sci. Technol., 50(21), 11779–11786, doi:10.1021/acs.est.6b02705, 2016.

Anonymous Referee #2

This study investigates the intra-regional transportation of black carbon (BC) between North China plain (NCP) and central China (CC) based on the simultaneously measurements at five cities located in the two regions during winter haze period. The authors have identified two important BC emission sources (i.e., biomass burning and fossil fuel) and their geographic origins during transportation. Since there are still limited studies on the intra-region transportation in China, this study takes insight in this topic. The manuscript is well written and organized. But there are still some minor issues, which need to be addressed before publication. Please see specific comments below.

AR: Thanks for your positive comments on this manuscript.

1. Lines 240-246: Taking the fossil fuel BC (BC_{ff}) as the control priority in WH and other cities in this study is not just because the BC_{ff} increases from clean to pollution period but also due to the much higher absolute conc. of BC_{ff} than biomass burning BC (BC_{bb}) under all the three conditions (Fig. 4b and c). Regarding Beijing case, in addition to the percentage of BC_{bb} increasing from clean to pollution episodes, are the absolute conc. of BCbb also higher than BC_{ff}? If not, it should be careful to state that the priority in North China is to control BCbb.

AR: Thanks for your comments and we have revised corresponding part. You concerns whether the absolute concentration of BC_{bb} was higher than BC_{ff} during pollution episodes in Beijing (Liu et al., 2018), the answer is yes as shown in Fig. R6. BC source apportionment using carbon isotope also suggests that BC emissions in BTH (North China) and PRD (South China) are characterized by coal-combustion-dominated and liquid fossil-combustion-dominated, respectively (Yu et al., 2018). This result supported our conclusion.

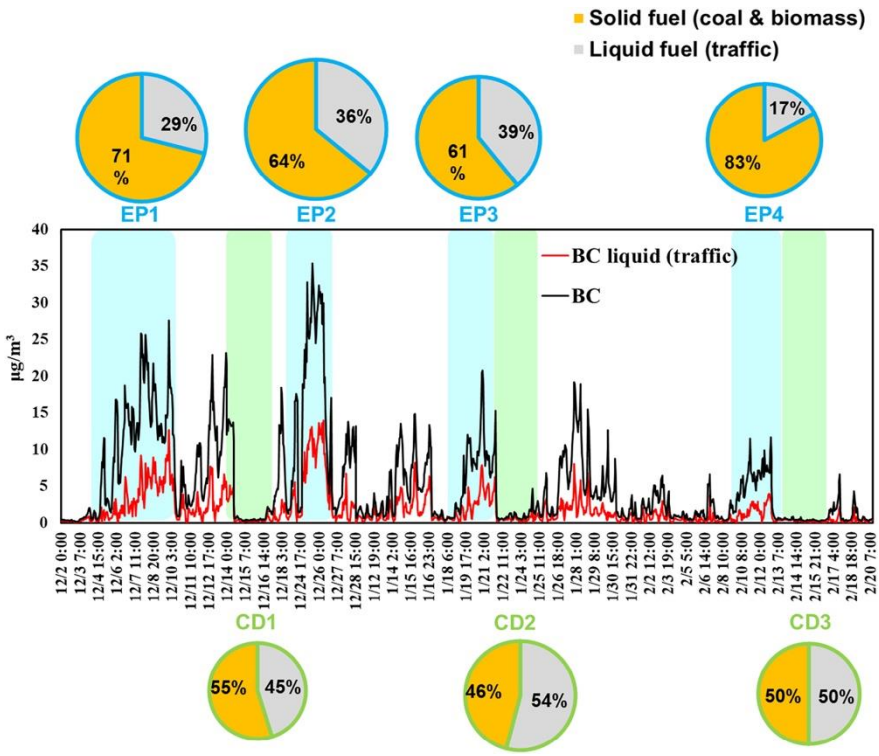

Figure. R6 Liquid and solid fuel source contributions to BC in pollution episodes (EP) and clean days (CD). The size of pies is proportional to average concentration of BC in each episode (Liu et al., 2018).

References

Liu, Y., Yan, C. and Zheng, M.: Source apportionment of black carbon during winter in Beijing, Science of The Total Environment, 618, 531–541, doi:10.1016/j.scitotenv.2017.11.053, 2018.

Yu, K., Xing, Z., Huang, X., Deng, J., Andersson, A., Fang, W., Gustafsson, Ö., Zhou, J. and Du, K.: Characterizing and sourcing ambient $PM_{2.5}$ over key emission regions in China III: Carbon isotope based source apportionment of black carbon, Atmospheric Environment, 177, 12–17, doi:10.1016/j.atmosenv.2018.01.009, 2018.

2. The aging process could significantly change the optical properties of BC aerosols (Peng J, et al., PNAS, 2016; Wang et al., J. Adv. Model Earth Syst, 2018). Are there any observed changes in BC absorption due to the aging during the intra-regional transportation?

AR: Thanks for your suggestion. We have observed the enhancement of BC absorption during the transportation according to two cases as shown in Fig. R7. In case 1, σ_{abs} significantly ($p<0.01$) increased from 25.6 ± 0.81 Mm^{-1} (LH) to 61.8 ± 12.5 Mm^{-1} (HA). In case 2, the enhancement of σ_{abs} was also observed from HA (53.4 ± 5.58 Mm^{-1}) to LH (59.9 ± 2.05 Mm^{-1}).

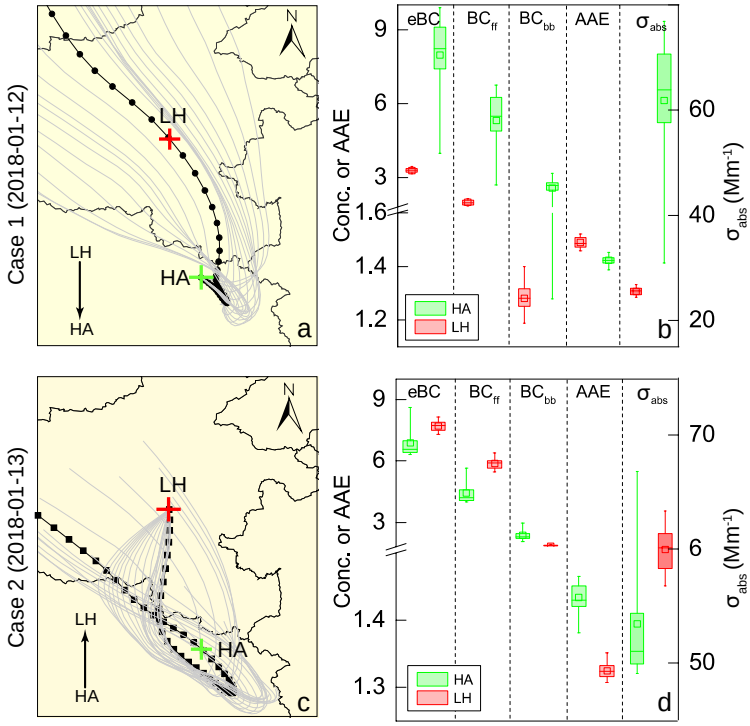

Figure. R7 Case studies of BC variation during the transportation from upwind to downwind direction. a (case 1): Hourly backward trajectories (grey line) reaching at HA on 2018-1-12 and the trajectory at 13:00 (GMT) (black line) was found passing through LH about 28 hours ago. c (case 2): Trajectory reaching at LH on 2018-1-13 07:00 (GMT) (black line) was found passing through HA about 31 hours ago. Box (25-75th percentiles) and whisker (5-95th percentiles) plots of eBC, BC_{ff}, BC_{bb} σ_{abs}, and AAE variations during the transport from LH to HA (b) and from HA to LH (d).

3. Fig.1: For air mass clustering panels, you may want to use different colors to differentiate the air masses from different directions.

AR: Thanks for your suggestions and we have corrected it (Fig. R8).

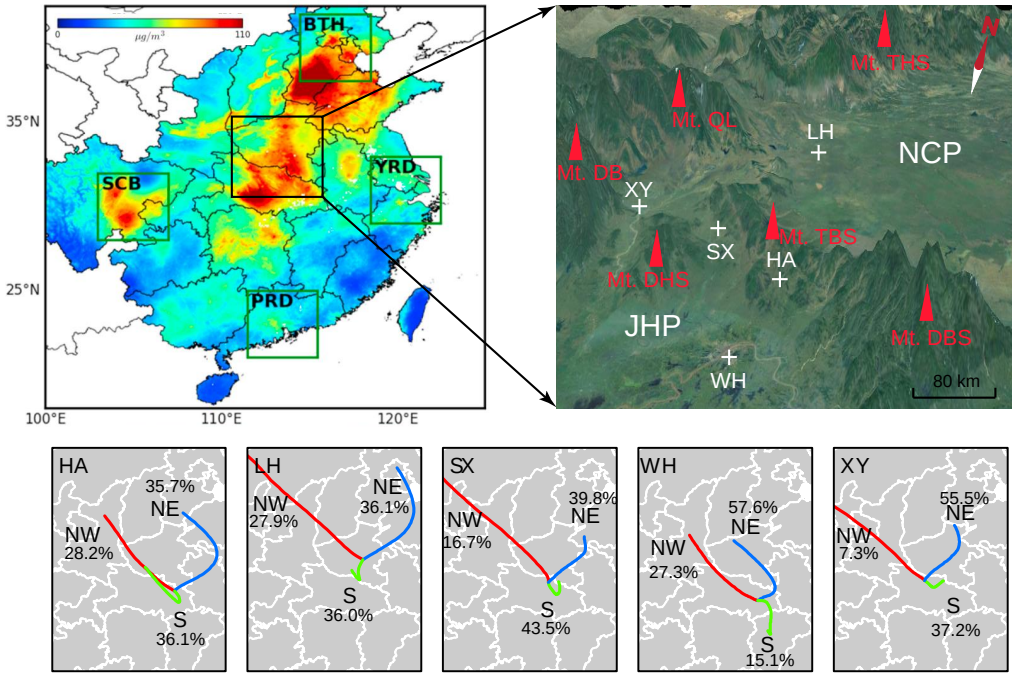

Figure. R8 Location, terrain of the study area and clusters of backward trajectories reaching at each observation site. Up left is the spatial distribution of the 15 years average $PM_{2.5}$ concentrations at a resolution of 1 km (Lin et al., 2018). Right up shows that the study area is surrounded by mountains and Mt. DBS and Mt. TBS blocks the North China Plain (NCP) and Jianghan Plian (JHP). Bottom shows that air masses reaching at the five sites were mainly from north directions (northwest and northeast) during the observation period.

4. Fig. 3: Does the count (y axis) denote the number of data points? If so, why there is much less data points at WH? The smaller total count might be because missing or not available data in measurements at WH?

AR: Yes, the y axis represents the number of data, the reasons why the number of data in WH ls less than other sites is due to the following two reasons: (1) there were much more missing values due to the instrument maintaining and power failure (2) the data resolution is 5-min at WH (AE31) and the resolution is 1-min at LH and HA (AE33).

5. Typos Line 227: Figure 3 is Figure 3b.

AR: Thanks, and it has been corrected.

Intra-regional transport of black carbon between the south edge of North China Plain and Central China during winter haze episodes

Huang Zheng[1, 2], Shaofei Kong[1], Fangqi Wu[1], Yi Cheng[1], Zhenzhen Niu[1], Shurui Zheng[1], Guowei Yang[1], Liquan Yao[2], Qin Yan[1,2], Jian Wu[1,2], Mingming Zheng[2,3], Nan Chen[3], Ke Xu[3], Yingying Yan[1], Dantong Liu[4], Delong Zhao[5], Tianliang Zhao[6], Yongqing Bai[7], Shuanglin Li[1], and Shihua Qi[2]

[1]Department of Atmospheric Science, School of Environmental Sciences, China University of Geosciences, Wuhan, 430074, China

[2]Department of Environmental Science and Technology, School of Environmental Sciences, China University of Geosciences, Wuhan, 430074, China

[3]Hubei Provincial Environmental Monitoring Centre, Wuhan, 430072, China

[4] Department of Atmospheric Sciences, School of Earth Sciences, Zhejiang University, Hangzhou, 310058, China~~School of Earth, Atmospheric & Environmental Sciences, University of Manchester, M139PL, UK~~

[5]Beijing Weather Modification Office, Beijing, 100089, China

[6]School of Atmospheric Physics, Nanjing University of Information Science and Technology, Nanjing, 210044, China

[7]Hubei Key Laboratory for Heavy Rain Monitoring and Warning Research, Institute of Heavy Rain, China Meteorological Administration, Wuhan, 430205, China

Correspondence to: Shaofei Kong (kongshaofei@cug.edu.cn)

Abstract. Black carbon (BC), from the incomplete combustion sources (mainly fossil fuel, biofuel and open biomass burning), is chemically inertness and optical ~~absorbance~~ absorber in the atmosphere. It has significant impacts on global climate, regional air quality, and human health. During the transportation, its physical-chemical characteristics~~, optical properties~~ and sources would change dramatically. To investigate the BC properties (i.e., mass concentration, sources and optical properties) during the intra-regional transport between the south edge of North China Plain (SE-NCP) and Central China (CC), simultaneous observations of BC at a megacity (Wuhan, WH) in CC, three borderline cities (Xiangyang, XY, Suixian, SX and Hong'an, HA, distributing from the west to east) between SE-NCP and CC and a city (Luohe, LH) in SE-NCP were conducted during the typical winter haze episodes. Using Aethalometer, the highest equivalent BC (eBC) mass concentration~~s~~ and aerosol absorption coefficients (σ_{abs}) were found in ~~the city (~~LH~~)~~ at SE-NCP, followed by the borderline cities (XY, SX and HA) and ~~megacity (~~WH~~)~~. The levels, sources, optical properties (i.e., σ_{abs} and absorption Ångström exponent, AAE) and geographic origins of eBC were different between clean and pollution episodes. Compared to clean days, ~~the~~ higher eBC levels (increased

by 26.4−163%) and σ_{abs} (increased by 18.2−236%) were found during pollution episodes due to more combustion of fossil fuel (~~contributing for~~increased by 51.1−277%), supported by the decreased AAE (by 7.40−12.7%). ~~Non-parametric wind regression~~Conditional bivariate probability function (CBPF~~NWR~~) and concentration-weighted trajectory (CWT) results showed that the geographic origins of biomass burning (BC_{bb}) and fossil fuel (BC_{ff}) combustion derived BC were different. ~~Based on cluster analysis of trajectories, a~~Air parcels from south direction dominated for border sites during clean days, with contributions of 46.0−58.2%, while trajectories from the northeast had higher contributions (37.5−51.2%) during pollution episodes. At the SE-NCP site (LH), transboundary influences from south direction (CC) exhibited more frequent impact (with the air parcels from this direction contributed 47.8% of all the parcels) on the ambient eBC levels during pollution episodes. At WH, eBC was mainly from the northeast transport route during the whole observation period. Two transportation cases showed that from upwind to downwind direction, the mass concentrations of eBC, ~~BC_{bb} and~~ BC_{ff},and σ_{abs} all increased, while AAE decreased. This study highlighted that intra-regional prevention and control for dominated sources at each~~of~~ specific site~~s~~ should be considered to improve the regional air quality.

1 Introduction

Black carbon (BC), a distinct type of carbonaceous material, has attracted ~~much~~ wide attention mainly due to its climate effect~~s~~ over past decades (Hansen et al., 2000; Jacobson, 2000; Bond et al., 2013). BC can strongly absorb but reflect less ~~visible~~ light and the direct radiative forcing is estimated to be +0.88 W m^{-2} (Bond et al., 2013). It is composed of small carbon spherules and has large specific surface areas, which allows it to absorb aerosol, and provide substrate for atmospheric chemical reactions (Liu et al., 2018a). BC also has adverse human health effect~~s~~ ~~(Jansen et al., 2005; Cao et al., 2012)~~ due to its absorption of carcinogenic pollutants (Jansen et al., 2005; Cao et al., 2012). Additionally, recent studies showed that BC can strongly impact the ambient air quality. For instance, in urban areas, BC can enhance ~~the~~ haze pollution by modifying the planetary layer height, which was unfavorable to the vertical dispersion of air pollutants (Ding et al., 2016). This “dome effect” is more substantial in rural areas under the same BC conditions (Wang et al., 2018a). BC particle, coated with more materials can markedly amplify absorption and direct radioactive forcing, which would further worsen the air quality (Peng et al., 2016; Liu et al., 2017a; Zhang et al., 2018). As the transportation key ~~point~~note~~s~~, the properties of BC at rural and suburban sites needed to be emphasized, which ~~is~~were always ignored in former field campaigns.

BC is formed only in combustion processes of carbon-based materials such as biomass and fossil fuels. The broadly reported BC sources can be grouped into stationary sources (i.e., industrial emission), area sources such as residential coal/wood combustion, open burning and mobile sources including diesel engines, etc. (Chow et al., 2011; Bond et al., 2013). To identify ~~the~~ BC sources, several methods including aethalometer model, diagnosis ratios and radioactive carbon isotope have been developed (Sandradewi et al., 2008; Verma et al., 2010; Zotter et al., 2016). Chow et al., (2011) summarized the ratios of element carbon to $PM_{2.5}$ (expressed as percentage, %) from various sources and these ratios have been used to qualitatively describe the BC sources (Liu et al., 2018a). Radiocarbon method can give the quantified results of BC sources as the

abundances of $^{14}C/^{12}C$ in fossil fuel and modern carbon sources (i.e., biogenic sources) are different. Radiocarbon method coupled with laevoglucose, a tracer of biomass burning ~~have~~ has been adopted in BC source apportionment (Zhang et al., 2015a; Liu et al., 2017b; Mouteva. et al., 2017; Salma et al., 2017). However, the technical limitations and the high cost for ^{14}C measurement block the application of radiocarbon method ~~to~~ in BC source apportionment. The aethalometer model is an alternative method, which can attribute the BC to fossil fuel combustion and biomass burning. The source apportionment can be conducted using multi-wavelength~~s~~ BC data (Sandradewi et al., 2008; Liu et al., 2018a) and the validity was proved by ^{14}C method (Zotter et al., 2016). Compared to other methods, aethalometer model can provide high-time resolution variation of BC source contributions (Kalogridis et al., 2017; Liu et al., 2018a), which can help to understand the atmospheric behaviors of BC, especial for the temporal variation~~s~~.

Atmospheric lifetime of BC varied from a few days to weeks and therefore, BC undergoes regional and intercontinental transport (Bond et al., 2013). During the transport, its mixing state, morphology and optical properties will change (China et al., 2015). As a result, BC has been observed in remote areas such as the polar regions (Huang et al., 2010; Weller et al., 2013; Qi et al., 2017; Xu et al., 2017) and Tibetan Plateau (Cong et al., 2013). ~~For instance,~~ Qi et al., (2017) found that Asian anthropogenic activities ~~contributed 35−45%~~ and biomass burning emissions from Siberian contributed 35−45% and 46−64%, respectively ~~–~~to the sources of BC in Arctic in April 2008 by GEOS-Chem modeling. ~~Similarly,~~ Xu et al. (2017) also used the global transport model to conclude that the anthropogenic emissions from eastern and southern Asia contributed most to the Arctic BC column loading with percentages being 56% and 37% for spring and annual, respectively. To study the regional transport of BC, backward ~~trajectori~~trajectory~~es~~ and concentration-weighted trajectory (CWT) were ~~always~~ also employed (Huang et al., 2010; Wang et al., 2017a). ~~The ratio of BC/CO ratio was adopted to study the BC aging during the transport processes (Verma et al., 2010; Pan et al., 2011; Guo et al., 2017).~~ However, p~~P~~revious studies mostly focused on the impact of BC transportation on its physical-chemical properties ~~during aging~~ at a given site (e.g., a megacity or a remote background site). A recent study indicated that in the south Ontario, higher BC loading in ~~the~~ summer was partly from the trans-boundary fossil fuel derived BC emissions in the US (Healy et al., 2017). To our knowledge, the interaction of BC transportation among various sites for a specific region has been rarely reported, which may limit the understanding of regional-joint control for air pollution.

After continuous efforts, especially in the last five years, the spatial distribution pattern of air pollution has changed obviously in China, and the positive result is that the average annual $PM_{2.5}$ concentration in Pearl River Delta (PRD) has achieved the national secondary standard level (http://www.zhb.gov.cn/hjzl/zghjzkgb/lnzghjzkgb/). Now the key regions suffering from severe $PM_{2.5}$ pollution are North China Plain (NCP), Yangtze River Delta (YRD), Sichuan Basin (SB), Fen-Wei River Basin and Central China (CC). From Lin et al. (2018), it could be found that the air pollution areas at the south edge of North China Plain (SE-NCP) and Central China were combined together and there existed obvious transportation routes between SE-NCP and CC. The spatial distribution of aerosol optical depth (AOD) across China also verified that high values existed in Central China (Tao et al., 2017). As an important chemical composition of $PM_{2.5}$, BC account for 7.1−25.3% ~~(Huang et al., 2014)~~ of $PM_{2.5}$ mass (Huang et al., 2014). ~~Despite a~~A lot of~~large scale~~ observations of ambient BC have~~s~~ been conducted (Table S1−S2)~~,~~

~~the BC studies~~ which are mainly ~~reported~~ for ~~in~~ NCP (Zhao et al., 2013; Ji et al., 2018; Liu et al., 2018~~ab~~; Wang et al., 2017a), YRD (Zhuang et al., 2014, 2015, 2017), PRD (Cheng et al., 2008; Wu et al., 2009; Wang et al., 2017b) and Tibetan Plateau (TP) (Zhu et al., 2017; Niu et al., 2018; Wang et al., 2018b). No studies have concerned the BC transportation and interaction between these key regions. BC emission inventory suggest~~ed~~s that there were differences in ~~different~~ source categories ~~exists~~ between NCP and CC (Wang et al., 2014~~ab~~; Qiu et al., 2016), especially for the residential coal combustion (Qin and Xie, 2012). It should be emphasized that during the winter period, there were central-heating activities in NCP, while no heating activities existed in Central China. It implied that the sources of BC should be ~~quite~~ different. Therefore, the special geographic locations and terrain of Central China (Fig. 1) ~~makes it complex but~~ provide an ideal opportunity to understand the BC levels, optical properties, sources and ~~their~~ its variation during intra-regional transportation between the two polluted regions. However, corresponding researches have not been reported.

Therefore, the aims of this study were to (1) study the differences of BC levels, sources, and optical properties under different air ~~pollution situation~~quality at this region; (2) quantify the regional transportation of BC at multiple observation sites in CC and SE-NCP. To study ~~the~~ BC sources, the diagnosis ratios and aethalometer model were used. The backward ~~trajectory based~~trajectory-based methods were employed to quantify the potential regional transport contribution. This paper firstly reported the sources of BC in Central China and gave the direct evidence of BC properties variation during the regional transportation between two key regions of China, which is helpful to develop effective countermeasures for mitigating regional air pollution.

2 Methodology

2.1 Observation plan

For ~~the~~ selecting the ~~sites~~site~~'~~s ~~selection~~, we refereed to the trajectory of air masses reached to Wuhan in~~for~~ January 2017 (Figure S1) and found that the north and northwest direction ~~were the main directions~~dominated. For the north direction, the air masses originated from~~at~~ the SE-NCP and Luohe is just on the north routes and close to the ~~origination~~ heavy polluted region as ~~the~~ Figure 1 shown. ~~Meanwhile, the~~ Central China is not an isolated region. From Figure 1, there were two obvious connection channels for $PM_{2.5}$ between SE-NCP and CC, which was decided by the mountains crossing the two regions. Therefore, to investigate the regional transport of air pollutants and also answer whether the pollutants in CC can be transported to SE-NCP in winter, five sites including WH, three borderline cities (Xiangyang, XY; Suixian, SX and Hong'an, HA, distributing from the west to east) between NCP and CC and a city (Luohe, LH) in SE-NCP were selected ~~as shown in Figure 1~~. The observation site at Wuhan locates on a rooftop of~~in the~~ Hubei Environmental Monitoring Centre, which is an urban site with no industrial emission sources. LH and XY sites are located in ~~the~~ suburban areas. HA and SX sites belong to rural areas. The observation instruments were placed near the local environmental monitoring stations. ~~and therefore, the s~~Six routine-monitored air pollutants including $PM_{2.5}$, PM_{10}, NO_2, SO_2, CO and O_3 were available. Black carbon measurement

instruments including Magee Scientific-AE31, AE33 and AE51 were deployed (Table 1). The observation periods started from 8th January after a regional snowfall event and ended at 25th January 2018 before another snowfall event coming. The observation duration at the five sites are summarized in Table 1.

2.2 Instrument description

AE31 continuously collects ~~the~~ ambient BC on ~~the~~ a quartz tape and measures ~~the~~ light singles on sampled spot (I) and reference spot (I_0) and the light attenuation (ATN) is defined as:

$$ATN = -100ln(\frac{I}{I_0}) \quad (1)$$

It assumes ~~the~~ a linear relation between BC mass loading and the delta of ATN as a result of BC deposited on the tape ~~is linear~~. ~~The~~ BC mass concentration is calculated as following:

$$BC = \frac{d(ATN)}{MAC} \times \frac{A}{V} \quad (2)$$

where MAC is the mass specific attenuation cross section ($m^2\ g^{-1}$); A is the area of sampled spot (1.67 cm^2); V is the volume of the sampled air passing through the tape. The disadvantage of AE31 is the filter loading effect, which needs further correction to compensate (Petit et al., 2015). The BC absorption coefficient (b_{abs}, Mm^{-1}) is calculated as:

$$b_{abs} = \frac{BC \times \mathrm{MAC}}{C \times R(ATN)} \quad (3)$$

where C is the calibration factor (2.14 for quartz material tape); R (ATN) is a correction factor for shadowing effect and it is empirically determined using the compensation parameter f (Weingartner et al., 2003):

$$\mathrm{R(ATN)} = \left(\frac{1}{f} - 1\right)\frac{\ln(ATN) - \ln(10)}{\ln(50) - \ln(10)} + 1 \quad (4)$$

To overcome the shortage of loading effect, AE33 (dual spot) was developed. It also simultaneously measures the ATN at seven wavelengths. Different to AE31, AE33 measures BC on two parallel spots on the fibre tape (Teflon-coated) with different flow rate:

$$BC_1 = BC \times (1 - k \cdot ATN_1) \quad (5)$$

$$BC_2 = BC \times (1 - k \cdot ATN_2) \quad (6)$$

The loading compensation k is calculated according ~~the~~ equation (5) and (6) and ~~the~~ BC mass concentration is further calculated as following:

$$\mathrm{BC} = \frac{A[d(ATN)/100]}{F_1(1-\varphi)MAC \cdot C(1-k\ ATN_1)dt} \quad (7)$$

For AE33, the area of sampled spot (A) is 0.785 cm^2 and enhancement parameter (C) is 1.57 for Teflon-coated fibre. The absorption coefficient (σ_{abs}, Mm^{-1}) by AE33 is estimated as multiplying BC mass concentration by MAC. More details about ~~the~~ BC concentration calculation, parameters (i.e., f and MAC for different wavelengths) and the differences between AE31 and AE33 can be found in previous study (Rajesh and Ramachandran, 2018). AE51 measures the absorbance (ATN) of the loaded spot (3 mm diameter) and the reference portion of ~~the~~ a Teflon-coated borosilicate glass fiber using a stabilized 880

nm LED light source. The flow rate of AE51 was set as 100 mL min^{-1} and more information about AE51 can be found online (https://aethlabs.com/microaeth/ae51/tech-specs).

2.3 Data processing

2.3.1 BC source apportionment

BC absorbs the solar spectrum efficiently with a weak dependence on wavelength and the absorption Ångström exponent (AAE) is used to describe this spectral dependence of absorption (Zhu et al., 2017). The AAE value varies significantly from one source to another, i.e., the AAE values for fossil fuel combustion and biomass burning derived BC are 1.0 and 2.0, respectively (Sandradewi et al., 2008). ~~Therefore, a~~ BC source apportionment method was established based on the AAE (Sandradewi et al., 2008) and was verified by ^{14}C method (Zotter et al., 2016).

Black carbon source apportionment using aethalometer model is based on the assumption that the aerosol absorption coefficient is different from fossil fuel combustion derived BC (BC_{ff}) and biomass burning derived BC (BC_{bb}). Because the absorption coefficients at different wavelengths are different and the absorption of BC_{ff} and BC_{bb} follow different spectral dependencies. The Ångström exponents: α_{ff} and α_{bb} are used to describe the dependencies of fossil fuel and biomass burning, respectively. The following equations are used ~~in BC source apportionment~~ (Sandradewi et al., 2008):

$$\frac{b_{abs}(470nm)_{ff}}{b_{abs}(950nm)_{ff}} = \left(\frac{470}{950}\right)^{-\alpha_{ff}} \quad (8)$$

$$\frac{b_{abs}(470nm)_{bb}}{b_{abs}(950nm)_{bb}} = \left(\frac{470}{950}\right)^{-\alpha_{bb}} \quad (9)$$

$$b_{abs}(470nm) = b_{abs}(470nm)_{ff} + b_{abs}(470nm)_{bb} \quad (10)$$

$$b_{abs}(950nm) = b_{abs}(950nm)_{ff} + b_{abs}(950nm)_{bb} \quad (11)$$

$$BB(\%) = \frac{b_{abs}(950nm)_{bb}}{b_{abs}(950nm)} \quad (12)$$

where b_{abs} (470 nm) and b_{abs} (950 nm) are ~~the black carbon~~BC absorption coefficients at 470 and 950 nm wavelengths, respectively. Due to the single channel (λ=880 nm) of AE51, BC source apportionment results were not available at SX and XY ~~and were only reported for HA, LH and WH~~.

2.3.2 Assessment of surface transport

Generally, the north wind dominated in winter in CC and air pollutants can be transported from upwind direction (north) to downwind direction (south). In order to evaluate the effects of regional transport, the surface transport under specific wind direction and speed per unit time was calculated according to ~~the~~ previous study (Wang et al., 2018b):

$$f = \frac{1}{n}\sum_{i=1}^{n} C_i \times WS_i \times cos\theta_i \quad (13)$$

where f stands for the surface flux intensity of BC (μg s^{-1} m^{-2}); n is the sum of observation hours; WS_i and C_i stand for the hourly average of wind speeds (m s^{-1}) and BC mass concentrations (μg m^{-3}) in the ith observation duration, respectively; θ_i

represents the angle differences between hourly wind direction and the defined transport directions (i.e., northwest-southeast for HA, SX and WH and north-south direction for LH and XY).

2.4 Potential geographic origins

The concentration-weighted trajectory (CWT) is always used to assess the regional transport of air pollutants (Kong et al., 2018; Zheng et al., 2018). This method is based on backward trajectory analysis. Prior to CWT analyses, the backward trajectory calculating was firstly conducted in each sampling site. The input wind datasets ~~into~~ for HYSPLIT are downloaded from the Nation Oceanic Atmospheric Administration (NOAA) (ftp://arlftp.arlhq.noaa.gov/pub/archives/gdas1/). For backward trajectory analysis, the air masses reaching at each observation site during the sampling period were calculated for 24 times with 1-hour resolution each day (starting from 0:00 to 23:00) at 200 m AGL (Fig. S2). These trajectories were than clustered according to their geographic origins (Fig. 1). For CWT analysis, a user-friendly tool Zefir written in Igor was used (Petit et al., 2017a). The domain covered by trajectories was divided into thousands of cells with 0.2° × 0.2°. More description about CWT can be found in text S1.

2.5 Auxiliary dataset

Hourly meteorological dataset including sea level pressure, temperature, relative humidity, wind speed, wind direction and visibility were acquired form the China Meteorological Data Service Centre (CMDC) (http://data.cma.cn, last accessed: 2018/1/26). The every 3-hour boundary layer height (BLH) was acquired from the NOAA's READY Archived Meteorology online calculating program (http://ready.arl.noaa.gov/READYamet.php, last accessed: 2018/4/8). Figure S3 shows the hourly averaged meteorological parameters at the five sites. ~~The m~~Meteorological conditions at the five sites followed ~~the same~~similar variation trends. However, significant differences ($p < 0.01$) of these parameters were found (Table S3). For instance, the average pressure, temperature and relative humidity at WH were significant higher ($p < 0.01$) than those at LH. For BLH, the mean values of the five sites showed insignificant differences.

~~As mentioned in section 2.1, the five observation sites were located next to the local air quality monitoring stations and therefore, s~~Six air pollutants (PM_{10}, $PM_{2.5}$, SO_2, NO_2, CO and O_3) were available and the data were downloaded from the China Environmental Monitoring Centre (http://www.cnemc.cn, last accessed: 2018/4/10). Figure S4 shows their hourly ~~average of six air pollutants at the five sites during~~variations during the observation period~~s~~. The major air pollutant was $PM_{2.5}$ during the entire ~~research~~ observation campaign. According to the Ambient Air Quality Standards (GB3095-2012), the air quality can be classified into clean, light polluted and heavily polluted when $PM_{2.5}$ mass concentrations are less than 75, between 75−250 and greater than 250 μg m^{-3}, respectively. Similar air quality classification was also reported elsewhere (Zheng et al., 2015; Zhang et al., 2018). Detailed information about the daily air quality of each site is shown in Fig. S5.

3 Results and discussion

3.1 General characteristics

Time series and box plots of the eBC concentrations (measured at 880 nm) at the five sites are shown in Fig. 2. The highest eBC concentrations was~~ere~~ observed at LH (8.48 ± 4.83 μg m^{-3}), followed by XY (7.35 ± 3.45 μg m^{-3}), HA (5.54 ± 2.59 μg m^{-3}), SX (4.47 ± 2.90 μg m^{-3}), and WH~~uhan~~ (3.91 ± 1.86 μg m^{-3}). As ~~the~~ Table S1 shown~~s~~, ~~Despite tthe sampling observation periods, site types, inlet of aerosol and instruments were different between different studies (Table S1),~~ BC was generally higher in North China and lower BC levels were found in remote areas and coastal areas as Fig. 3a shows. ~~For instance,~~ Wang et al, (2014b) analyzed ambient BC in an urban site in Xi'an during winter and found the average mass concentration was 8.8 ± 3.7 μg m^{-3}, which was higher than that in this study. Compared to other regions, ~~the~~ BC levels in this study were higher than a remote area of Lulang in southeastern part of the Tibetan Plateau (0.31 ± 0.55 μg m^{-3}) ~~reported by (~~Wang et al., ~~,(~~2018) as well as coastal areas such as Hong Kong (1.4 ± 1.1 μg m^{-3}) (Wang et al., 2017a) and a rural site in Shenzhen (2.6 ± 1.0 μg m^{-3}) (Huang et al., 2012). From BC emission inventory, North and Central China hold higher BC emission intensity (Qin and Xie, 2012; Yang et al., 2017)~~, i.e., ~~. E~~emission ~~rates~~ amounts in Hubei and Henan provinces were about 0.6−1.0 g C m^{-2} yr^{-1}, which were higher than other regions (Yang et al., 2017). Simulation results also suggested that the near-surface concentrations of BC (6−8 μg m^{-3}) in Hubei and Henan were higher than those in south China (4−6 μg m^{-3}) during winter (Yang et al., 2017). Compared to the ~~results~~data in other countries (Table S1), BC levels in this study were higher than those in Finland (Hyvärinen et al., 2011), France (Petit et al., 2017b), Ontario (Healy et al., 2017), and south Africa (Chiloane et al., 2017).

For the aerosol absorption properties measured at seven wavelengths by aethalometer, the characteristics (i.e., temporal variation) are generally consistent with each other and the corresponding properties for wavelength at 520 nm is mostly discussed (Zhuang et al., 2015, 2017; Wang et al., 2017b). T~~herefore, hen,~~ we only discussed the absorption properties at λ = 520 nm. Figure ~~43~~a ~~shows~~show the frequency distribution of absorption coefficients (σ_{abs}) at ~~various~~ three sites. σ_{abs} measured at HA, LH, and WH exhibited a single peak pattern. The average values of σ_{abs} measured at HA, LH and WH were 86.0, 132 and 60.6 Mm^{-1}, respectively. Similar to the spatial distribution of BC level~~s~~, higher σ_{abs} was found in North and Central China, while lower values observed in coastal areas and Tibetan Plateau (Fig. 3b and Table S2).

Figure ~~43~~b also shows the average absorption spectra measured at seven wavelengths for different sites. The power law fit was used to calculate the AAE (Zhu et al., 2017). The highest average AAE value was found at LH (1.37~~40~~), followed by HA (1.32) and WH (1.29~~34~~)~~– and HA (1.32)~~. The results indicated that the AAE was different at urban, suburban and rural sites. Generally, the AAE from coal combustion (2.11−3.18) (Sun et al., 2017) and biomass burning (1.85−2.0) (Petit et al., 2017b) were higher than that from traffic sources (0.8−1.1) (Sandradewi et al., 2008; Olson et al., 2015). Therefore, AAE at~~in~~ different sites suggested the different energy consumption structure and more coal or biomass were burned in North China (i.e., LH in this study).

3.2 Clean days *vs* pollution episodes

Figure. 54 shows the eBC concentrations under different air~~–~~ qualitypollution situation. It clearly shows that the eBC concentrations increased as the deterioration of air quality. ~~For instance, a~~At LH, the average eBC concentrations were 3.39 ± 2.06 μg m^{-3}, 8.31 ± 4.55 μg m^{-3} and 13.0 ± 4.59 μg m^{-3}, respectively when the air quality was clean, light polluted and heavy polluted. The average values of eBC increased by 163%, 139%, 96.2%, 51.8% and 26.4% at SX, XY, LH, HA and WH, respectively from clean to pollution. The eBC enhancement ~~of eBC~~ along with the ~~deterioration of~~ air quality deterioration was also reported elsewhere (Wang et al., 2014b, c~~a~~; Liu et al., 2016, 2018a~~b~~). At LH and HA, the enhancement of eBC level from clean to pollution period was due to both the elevated BC emissions from biomass burning (BC_{bb}) and fossil fuel combustion (BC_{ff}) (Fig. 54b and 54c). The BC_{ff} accounted for a higher contribution to eBC and the percentages of BC_{bb} to eBC decreased during the haze episodes (Fig. 4d). At WH, both the concentration and percentage of BC_{bb} ~~both~~ decreased from clean to pollution, which suggested that more BC_{ff} was emitted during haze episodes. This finding was different with previous study conducted in Beijing that the absolute concentration and percentage of ~~BC_{bb}~~ biomass burning and coal combustion ~~to eBC~~ were higher than traffic source to eBC and increased from clean to pollution episodes (Liu et al., 2018a~~b~~). The differences suggested that the control of fossil fuel combustion (vehicle emissions) instead of coal or biomass burning should be taken priority during the haze episodes at~~in~~ WH. While it should give priority to biomass and coal combustion control in North China to prevent air pollution.

Additionally, the aerosol optical properties (σ_{abs} and AAE) also exhibited different levels under different air qualitypollution ~~situation~~. Similar to eBC levels, the σ_{abs} ~~also~~ elevated by 11.7−254% as the air quality switched from clean to pollution (Fig. 54e). Our observation (Fig. S6) and previous study found that t~~T~~here are more secondary aerosols (i.e., sulfate, nitrate) during the pollution episodes (Huang et al., 2014)~~., and~~ T~~t~~he increased secondary aerosols would be more adsorbed on ~~the surface of~~ BC particle and therefore, the BC absorption ~~. The absorption of BC therefore~~ enhanced via the lens effects of these coated materials (Jacobson, 2000; Moffet and Prather, 2009). On the contrary, the AAE showed higher values during clean days when compared to pollution episodes (Fig. 54f). The AAE decreasing ~~of AAE~~ from clean to polluted days was also reported elsewhere (Zhang et al., 2015b) and it can be partly attributed to the source variation. ~~For instance, t~~The AAE for biomass burning is about 2.0 while the AAE for fossil fuel combustion is about 1.0 (Sandradewi et al., 2008). Higher AAE values during clean days suggested that more BC ~~was~~ may be from biomass burning and lower AAE indicated the dominance of fossil fuel combustion during the pollution period (Fig. 54c). The AAE is also sensitive to other factors such as the particle size. Previous studies suggested that the particle diameter and number concentration increased from clean to pollution episodes due to several factors such as coagulation, hygroscopic growth, emissions, meteorological conditions, i.e., planetary boundary layer and wind speed (Guo et al., 2014; Zhang et al., 2017). These studies suggested that the particle diameter is generally larger during pollution days. Furthermore, the lab combustion and numeric simulation proved that ~~black carbon~~BC particle with larger geometric median diameter had lower AAE value (Singh et al., 2016; Liu et al., 2018b). Therefore, lower AAE was observed during pollution episodes in this study.

Figure 6~~5~~ and Fig. S7 shows the diurnal variations of eBC and absorption coefficients under different air quality. The diurnal cycles of black carbon and absorption showed similar variation patterns. T~~and we discussed t~~he BC mass concentrations were discussed here. At HA, LH and SX, after sunrise, an increasing and a peak value at about 09:00 local time (LT) were observed. This variation was more obvious during pollution days due to the higher eBC levels. The morning peak may be related with the combined effects of increased biomass burning and fossil fuel combustion emissions (Fig. S7~~6~~). Additionally, the low mixing layer height in the morning also favored the accumulation of eBC. After sunrise, with the elevation of BLH, the eBC levels decreased and the minimum occurred at about 15:00 (LT). In the evening hours, eBC showed increasing trend~~s~~ and peake~~ds~~ at about 21:00 (LT). ~~The same~~Similar diurnal patterns of eBC were also reported in other areas (Verma et al., 2010; Ji et al., 2017; Liu et al., 2018a~~b~~). However, the diurnal variations of eBC at WH and XY exhibited different patterns during clean or pollution episodes. The diurnal pattern of eBC at WH was not likely controlled by the development of mixing layer height, which may lead to the maximum and minimum values of air pollutants generally occurring at sunrise and afternoon, respectively. The unexpected lower value in the morning (about 09:00 LT) and higher value in the afternoon (15:00 LT)~~,~~ at WH needed~~s~~ further research.

3.3 Ratios of BC/$PM_{2.5}$ and BC/CO

The BC/$PM_{2.5}$ and BC/CO ratios are widely used to identify the BC sources (Zhang et al., 2009; Wang et al., 2011; Verma et al., 2010; Chow et al., 2011). Generally, the ratios of BC/$PM_{2.5}$ from ~~oil combustion (traffic)~~mobile sources (0.059-0.74) and area sources (0.032-0.33) were higher than that from industrial sources (0.0046-0.03) ~~and agricultural burning are higher than those from industrial emissions such as manufacturing and mineral products~~. For instance, the mobile sources hold the highest ratios of BC/$PM_{2.5}$ (0.33−0.77) and the ~~residential wood combustion~~cement kiln showe~~ds~~ lower ratio (0.03~~56~~) (Chow et al., 2011). For the BC/CO ratios (μg m^{-3}/ppbv), it also varied ~~from~~ for different sources, i.e., traffic (0.0052), industry (0.0072), power plant (0.0177), and residential (0.0371) (Zhang et al., 2009). In this study, the BC, $PM_{2.5}$ and CO were well correlated with each other (Fig. S8~~7~~). The correlation coefficients (r^2) between BC and $PM_{2.5}$ were 0.67, 0.30, 0.44, 0.37 and 0.48 at LH, HA, WH, SX and XY, respectively. Significant correlations ($p < 0.05$) between BC and CO were found with r^2 ranging from 0.27 (XY) to 0.71 (LH). The good correlations indicated that the BC, $PM_{2.5}$ and CO may be from similar sources (except HA with low r value as 0.06).

Overall, BC in this study was not likely from industrial emissions (Fig. 7~~6~~a), as the BC/$PM_{2.5}$ ratios (μg m^{-3}/μg m^{-3}) ~~in this study~~ (0.045−0.083) were higher than those from industry (0.0046−0.03) (Chow et al., 2011). Instead, BC/$PM_{2.5}$ ratios at the five sites were all within the range of oil combustion (0.03−0.136). Additionally, the BC/$PM_{2.5}$ ratios at LH and SX were in line with the ratio from residential wood combustion. From BC/CO ratios, BC was more likely from biomass burning (crop residue: 0.0056−0.016) at HA and LH, while it was mainly from gasoline combustion in SX, WH, and XY (Fig. 7~~6~~b). Quantified calculation results using equations in section 2.3.1 also suggested that the fractions of BC from biomass burning at HA (27.6 ± 9.40%) and LH (29.5 ± 9.14%) were significant higher ($p < 0.01$) than that at WH (25.4 ± 11.8%). Compared to other urban areas, the ratios of BC/CO (μg m^{-3}/ppbv) at SX (0.004), and WH (0.0044) were lower than those in Beijing (0.0058)

(Han et al., 2009), Guangzhou (0.0054) (Verma et al., 2010), Gwanjun (0.006) (Park et al, 2005) and Tokyo (0.0057) (Kondo et al., 2006) as well as Mt. Huang (0.0065) (Pan et al., 2011), while ratios at HA (0.0091) and LH (0.0076) were higher than the values in ~~–~~these studies.

~~Due to the longer atmospheric lifetime of CO, the ratio of BC to CO and the correlation coefficients of them would decreased from upwind to downwind directions (Guo et al., 2017). Therefore, the BC/CO is used to reflect the BC aging during the transport (McMeeking et al., 2010; Verma et al., 2010; Guo et al., 2017). Table 2 summarizes the BC/CO ratios at different observation sites under different air pollution situation. Except for WH, clean days held significant lower BC/CO ratios than those during the pollution episodes ($p < 0.01$). For instance, at LH, the BC/CO ratio during clean days (0.0058 ± 0.0024 μg m^{-3}/ppbv) was significant lower ($p < 0.01$) than heavy pollution episodes (0.0071 ± 0.0013 μg m^{-3}/ppbv). The coefficients (r^2) also decreased from pollution (0.52) to clean days (0.27). The BC/CO ratios suggested that when the air quality was good, BC was more aged while it was fresher during the pollution episodes.~~

3.4 BC under different wind direction and speed

~~Nonparametric wind regression (NWR)~~Conditional bivariate probability function (CBPF) plot was used to identify and quantify the impact of likely source regions of air pollutants as defined by wind direction and speed ~~–~~(Carslaw and Ropkins, 2012)~~(Henry et al., 2009)~~. Fig. S~~9~~8 shows the eBC levels under different wind speed and directions at the five sites. As shown in Fig. 1, SX and HA are located in the northwest direction of WH and ~~therefore,~~ high eBC levels were found in the northwest directions of SX, HA and WH when north wind dominated. On the contrary, when the south wind dominated, BC was blowing from south to the north direction and high levels were found in the south direction at WH and HA. However, at LH and XY, higher levels of BC were only found from south direction. In addition to eBC levels, the BC_{bb} and BC_{ff} under different wind speed and directions were also discussed at HA, LH and WH (Fig. 8~~7~~). At HA, the ~~NWR~~ CBPF plot~~s~~ of BC_{ff} was in line with eBC and high levels were from both northwest and south directions while the high level of BC_{bb} (> 1.8 μg m^{-3}) was only found in southeast direction. ~~The same~~Similar result was also found at WH. High level of BC_{bb} was due to more biomass burning in the southeast direction of HA and WH (Fig. S10). At LH, the ~~NWR~~ CBPF plots of BC_{bb} and BC_{ff} were the same with the eBC as discussed above.

In order to describe the BC transportation from upwind to downwind directions, we used Eq. (13~~6~~) in section 2.3.3 to calculate the surface transport (ST) of eBC (Fig. 9~~8~~). The calculated average S~~A~~T values of BC were −0.69 ± 10.2, −0.06 ± 12.0, −0.17 ± 5.33, 0.29 ± 6.14 and 0.99 ± 17.8 μg s^{-1} m^{-2}, respectively for HA, LH, SX, WH and XY. The negative values at HA, LH and SX suggested that the transportation intensity of BC from south (southeast) to north (northwest) direction was higher, while the positive values observed at WH and XY indicated that more BC was transported from north direction to south direction. The large standard deviation of SAT reflected strong fluctuations in transport, which was due to wind speed, directions and BC levels (Wang et al., 2018b).

3.5 Potential geographic origins

Employing CWT method, the potential geographic origins of eBC for the five sites were explored (Fig. S119). Overall, CWT results of eBC at the five sites suggested that high eBC levels were found both in the north and south directions of LH and WH, while the high levels (i.e., > 4 μg m^{-3}) of eBC were only found from northeast directions of HA, SX and XY (Fig. S119). ~~In addition to the~~Additionally, ~~possible geographic origins of eBC,~~ the potential geographic source regions of BC_{bb} and BC_{ff} at HA, LH and WH were also discussed as shown in Fig. 10. At HA, the CWT results showed that high levels of eBC (i.e., > 3 μg m^{-3}) were from north-/northeast direction. However, the hot spots of BC_{bb} and BC_{ff} were different, with higher levels of BC_{bb} from both south and north directions and higher levels of BC_{ff} from the north direction~~. The hot spots of BC_{bb} and BC_{ff} occurring in the north of HA were likely due to the intensive BC emission in this area~~. Also, higher levels of BC_{bb} and BC_{ff} were found in the south of LH. Opposite to the CWT results at HA, the hot spots of BC_{bb} was only found in the southeast direction of WH and high levels of BC_{ff} were found in the north and south directions of WH. The CWT results at WH were in line with the ~~wind rose~~CBPF plots in section 3.4. The unity of CWT and ~~wind rose plots~~CBPF results at WH suggested that there were intensive biomass burning activities in the south direction of WH during the observation period, which was verified by the MODIS fire-points distribution (Fig. S10).

~~Furthermore, w~~We also discussed the source region differences of eBC under different air quality (Fig. 110). The higher levels (>1 μg m^{-3}) of eBC, BC_{bb} and BC_{ff} were mainly from the south direction of ~~HA~~ three sites when the air was clean.~~,~~ ~~W~~while during the pollution episodes, air parcels from the north direction contributed high concentrations~~. (> 3 μg m^{-3}) to the BC at HA~~. For instance, at WH, high levels of eBC (> 2.5 μg m^{-3}) were found from south direction, while the source regions with high level eBC (> 3 μg m^{-3}) switched to northeast direction when the air quality was worsened. Figure 12 shows the semiquantitative results of transportation contribution results during clean and pollution episodes. At the boundary sites (HA, SX and XY), BC was mainly from south direction (accounting for 46.0−58.2%) when the air quality was clean, and it was mainly from northeast/northwest directions (51.2−76.5%) when the air quality getting worse. At SE-NCP site (LH), BC was dominantly from south direction (47.8%) during pollution episodes~~ in this study~~. At CC site (WH), BC was mainly from northeast direction (49.3−71.1%). These results suggested that northwest and northeast directions were the main transport pathways of air pollutants reaching to WH during the pollution episodes. Furthermore, to control local emissions during haze episodes, the emission sources, i.e., industry plant and open biomass burning in the upwind direction should also be controlled to prevent the further deterioration of air quality in downwind areas.

~~The CWT plots of BC_{bb} and BC_{ff} showed similar distribution with eBC. At LH, CWT results of eBC, BC_{bb} and BC_{ff} showed that high levels of eBC were mainly from south direction during clean days. When the air quality degraded to pollution, the air masses from south and east directions both contributed to the high eBC (i.e., > 5 μg m^{-3} for BC) at LH. CWT results at WH showed that the southeast direction was the dominant source regions of eBC, BC_{bb} and BC_{ff} during clean days, while the source regions switched to northeast direction when the air quality changed into pollution.~~

~~To give quantified results of which cluster had greater contribution to eBC level at the receptor sites, the percentage contributions of each cluster reaching at the five sites under different air pollution situation are summarized in Figure 11. Trajectories from south was the main transport pathways reaching at HA, which accounted for 49.6% for clean days and therefore, the highest average eBC level (6.33±1.61 μg m^{-3}) was found from south direction during the clean days. However, the percentage contribution for the south cluster contributed least (21.4%) to the total air masses, but it had the highest eBC level (7.89±2.59 μg m^{-3}) among the three clusters during the pollution episode. At LH, despite the lowest ratio of trajectories were found from south (16.7%) and northwest (21.6%), respectively for clean and pollution days, these two clusters had the highest eBC levels. At WH, the cluster with the highest percentages also had the highest BC levels. For instance, northeast direction was the primary pathway of BC reaching at WH and the highest average eBC value was also found from this direction. In summary, at the boundary sites (HA, SX and XY), BC was mainly from south direction (accounting for 46.0–58.2%) when the air quality was clean and it was mainly from northeast/northwest directions (51.2–76.5%) when the air quality getting worse. At SE-NCP site (LH), BC was dominantly from south direction (47.8%) during pollution episodes in this study. At CC site (WH), BC was mainly from northeast direction (49.3–71.1%). These results suggested that northwest and northeast directions were the main transport pathways of air pollutant reaching to WH during the pollution episodes. Furthermore, in addition to control local emissions during haze episodes, the emission sources, i.e., industry plant and open biomass burning in the upwind direction should also be controlled to prevent the further deterioration of air quality.~~

3.6 Case studies for BC properties variation during transportation

To explore the BC variations (i.e., mass concentration, sources and AAE) during the transportation, we chose two cases. LH and HA were selected as the study sites due to the same instrument deployment (AE33) and they are representative of SE-NCP and CC. BC transportation from HA to LH and from LH to HA were both considered. Figure 1~~3~~2a ~~shows~~show the hourly backward trajectories reaching at HA on 2018-1-12 and the trajectory at 13:00 ~~(UTC)~~ (GMT) (black line) was found passing through LH ~~(black line)~~ and the travelling time was about 28 h. Therefore, the eBC mass concentration (including BC_{ff} and BC_{bb}), ~~,~~ σ_{abs} and AAE at the upwind site LH on 8:00 2018-1-11 (GMT) ~~,~~ and downwind site HA on 13:00, 2018-1-13 ~~(UTC)~~ (GMT) were compared (Fig. 13b). In case 1, d~~D~~uring the air transport from LH to HA, eBC, BC_{ff} ~~,~~ and BC_{bb} significantly increased ($p < 0.01$)~~,~~. ~~The black carbon~~ BC absorption enhancement from 25.6 ± 0.81 Mm^{-1} (LH) to 61.8 ± 12.5 Mm^{-1} (HA) was also observed, while the AAE significantly decreased from 1.49 ± 0.02 to 1.42 ± 0.02 ($p < 0.01$). Similarly, in case 2, the air masses reaching at LH on 7:00, 2018-1-13 ~~(UTC)~~ (GMT) were also passing through HA (black line) ~~before~~ about 31 h ago ~~(black line)~~ (Figure 1~~3~~2c). The eBC~~, and~~ BC_{ff} and σ_{abs} increased from upwind (HA) to downwind (LH), while BC_{bb} and AAE decreased from 2.37 ± 0.23 μg m^{-3} and 1.43 ± 0.02 to ~~1~~2.14 ± 0.14 μg m^{-3} and 1.32 ± 0.01, respectively (Fig. 13d). The eBC mass concentrations ~~were found~~ enhanced during the transportation regardless of the transport direction was from CC to NCP or from NCP to CC. Atmospheric removal of ~~black carbon~~BC occurs in a few days to weeks via wet and dry depositions or contact with surfaces (Bond et al., 2013). In these two cases, there were no precipitation events and the transport time was short (i.e., 28 and 31h), which suggested the less removal rates. Therefore, the new emission inputs along the trajectory

enhanced the eBC mass concentration during the transport. However, slight differences were found for BC_{bb} transport: BC_{bb} increased from north direction (LH: 1.28 ± 0.06 μg m^{-3}) to south direction (HA: 2.57 ± 0.47 μg m^{-3}), while BC_{bb} decreased from HA (2.37 ± 0.23 μg m^{-3}) to LH (2.14 ± 0.14 μg m^{-3}). The difference suggested that there were more intensive biomass burning emissions in Henan than Hubei province, which was also ~~proved~~verified by the BC emission inventory (Qin and Xie, 2012; Qiu et al., 2016).

Previous stud~~y~~ies found that the BC coagulation with non-refractory materials becomes more significant when the aging timescale was greater than 10 h (Riemer et al., 2004). ~~The c~~Chamber studies~~y~~ and field observations also found that the BC absorption enhancement under polluted urban ambient air (Peng et al., 2016, Zhang et al., 2018, Wang et al., 2018c), suggesting the role of aging in modifying ~~the~~ BC optical properties. In these two cases, the travelling time (aging time) from LH to HA and from HA to LH w~~ere~~as 28 h and 31 h, respectively, which suggested that the BC particle should be coagulated through complex atmospheric processes. Therefore, the σ_{abs} was found increased from upwind to downwind site. On the contrary, the AAE values were found decreased during the transport. The AAE is sensitive to the particle size. ~~For instance, t~~A~~he~~ lab combustion experiment showed that the particles with smaller diameter from fresh biomass burning have lower AAE value than larger particles (Singh et al., 2016). Simulation also confirmed that the AAE of BC particle decreased with the increasing of its geometric median diameter (Liu et al., 2018b). Therefore, the diameter of BC particle increased during the transportation due to the aging processes supported by the increased absorb coefficients and decreased AAE as discussed above~~The same result was also found through numerical simulation (Liu et al., 2018b). Additionally, chamber study of diesel soot particles coated with secondary organic compound also found that the AAE decreased from 1.13 to 0.8 (Schnaiter, 2005). The decreasing of AAE of BC particles during the transport indicated that BC was coated by other materials.the new emission inputs along the trajectory enhanced the eBC mass concentration during the transport.However, slight differences found for BC_{bb} transport: BC_{bb} increased from LH (1.28 ± 0.06 μg m^{-3}) to HA (2.57 ± 0.47 μg m^{-3}), while BC_{bb} decreased from HA (2.37 ± 0.23 μg m^{-3}) to LH (2.14 ± 0.14 μg m^{-3})~~.

4 Summary

In order to understand the levels, optical properties, sources, regional transportation and aging of BC in Central China and south edge of North China Plain during winter haze episodes, simultaneous observations at rural sites (HA and SX), suburban (LH and XY) and megacity (WH) were conducted during January 2018. Using the diagnosis ratios, aethalometer model, backward trajectory and concentration-weighted trajectory (CWT) methods, conclusions were drawn as following:

(1) Generally, the highest ambient eBC was found in northern sites (8.48 ± 4.83 μg m^{-3} and 7.35 ± 3.45 μg m^{-3} at LH and XY), followed by the transport route sites (5.54 ± 2.59 μg m^{-3} and 4.47 ± 2.90 μg m^{-3} for and HA and SX), and southern site (3.91 ± 1.86 μg m^{-3} for WH).

(2) Levels, sources, optical properties, and diurnal variation of eBC were different under different air quality. eBC concentrations and absorption coefficients (σ_{abs}) increased by 26.4−163% and 11.7−254~~%~~ %, respectively, from clean to

pollution episodes. The increasing may be due to more fossil fuel combustion emissions during pollution episodes, supported by lower Ångström exponent (AAE) and higher BC_{ff} concentrations.

(3) $BC/PM_{2.5}$ and BC/CO ratios suggested that BC was mainly from oil combustion and residential wood or biomass combustion in this region. ~~The higher BC/CO ratios during pollution episodes than those for clean days suggested that the BC particle was fresher during pollution days.~~

(4) ~~Nonparametric wind regression (NWR)~~Conditional bivariate probability function results of BC_{bb} and BC_{ff} showed different dominate source regions ~~with~~ of BC_{bb} (~~BC_{bb}~~ mainly from southeast direction) and BC_{ff} (from both northwest and southeast) of WH and HA. However, BC_{bb} and BC_{ff} were mainly from south direction of LH.

(5) At the boundary sites (HA, SX and XY), eBC was dominantly from south direction (accounting for 46.0−58.2%) when the air ~~quality~~ was ~~clean~~clean, and it was mainly from northeast/northwest directions (51.2−76.5%) during pollution episodes. At the SE-NCP site, air masses from south direction accounted for 47.8% of ambient BC level when the air was polluted. At the CC site, air parcels from northeast contributed 49.3−71.1% to the BC loading during the entire observation period ~~(i.e., clean days and pollution episodes)~~.

(6) During the air transportation from upwind to downwind direction, BC mass concentration and absorption coefficients increased, while the AAE decreased. This study firstly revealed the differences of levels, optical properties and sources of BC at five sites in south edge of North China Plain and Central China during winter haze episodes and discussed the interaction of BC between two key polluted regions. It was expected to be a demonstration for corresponding researches on regional interaction of BC transportation during winter haze episodes for other regions.

Data availability. Data is available on request to kongshaofei@cug.edu.cn.

Author contributions: HZ, SF K, TL Z, and SH Q designed the study; HZ and SF K wrote the paper; YY Y, DT L, DL Z, TL Z, YQ B, and SL L commented on this paper; MMZ, N C and K X provided the routine air pollutant data; others helped the field observation.

Acknowledgement. This study was financially supported by the Key Program of Ministry of Science and Technology of the People's Republic of China (2016YFA0602002; 2017YFC0212602), the Key Program for Technical Innovation of Hubei Province (2017ACA089) and the Program for Environmental Protection in Hubei Province (2017HB11). The research was also funded by the Start-up Foundation for Advanced Talents (201616) and the Fundamental Research Funds for the Central Universities (201802), China University of Geosciences, Wuhan.

References

Andreae, M. O. and Merlet, P.: Emission of trace gases and aerosols from biomass burning, Glob. Biogeochem. Cycles, 15(4), 955–966, doi:10.1029/2000GB001382, 2001.

Bond, T. C., Doherty, S. J., Fahey, D. W., Forster, P. M., Berntsen, T., DeAngelo, B. J., Flanner, M. G., Ghan, S., Kärcher, B., Koch, D., Kinne, S., Kondo, Y., Quinn, P. K., Sarofim, M. C., Schultz, M. G., Schulz, M., Venkataraman, C., Zhang, H., Zhang, S., Bellouin, N., Guttikunda, S. K., Hopke, P. K., Jacobson, M. Z., Kaiser, J. W., Klimont, Z., Lohmann, U., Schwarz, J. P., Shindell, D., Storelvmo, T., Warren, S. G. and Zender, C. S.: Bounding the role of black carbon in the climate system: A scientific assessment, J. Geophys. Res. Atmos., 118(11), 5380–5552, doi:10.1002/jgrd.50171, 2013.

Cao, G., Zhang, X., Gong, S. and Zheng, F.: Investigation on emission factors of particulate matter and gaseous pollutants from crop residue burning, J. Environ. Sci., 20(1), 50–55, doi:10.1016/S1001-0742(08)60007-8, 2008.

Cao, J., Xu, H., Xu, Q., Chen, B. and Kan, H.: Fine particulate matter constituents and cardiopulmonary mortality in a heavily polluted Chinese city, Environ. Health. Perspect., 120(3), 373–378, doi:10.1289/ehp.1103671, 2012.

Carslaw, D. C. and Ropkins, K.: openair — An R package for air quality data analysis, Environ. Model. Softw., 27–28, 52–61, doi:10.1016/j.envsoft.2011.09.008, 2012.

Cheng, Y. F., Wiedensohler, A., Eichler, H., Su, H., Gnauk, T., Brüggemann, E., Herrmann, H., Heintzenberg, J., Slanina, J. and Tuch, T.: Aerosol optical properties and related chemical apportionment at Xinken in Pearl River Delta of China, Atmos. Environ., 42(25), 6351–6372, doi:10.1016/j.atmosenv.2008.02.034, 2008.

Chiloane, K. E., Beukes, J. P., van Zyl, P. G., Maritz, P., Vakkari, V., Josipovic, M., Venter, A. D., Jaars, K., Tiitta, P., Kulmala, M., Wiedensohler, A., Liousse, C., Mkhatshwa, G. V., Ramandh, A. and Laakso, L.: Spatial, temporal and source contribution assessments of black carbon over the northern interior of South Africa, Atmos. Chem. Phys., 17(10), 6177–6196, doi:10.5194/acp-17-6177-2017, 2017.

China, S., Scarnato, B., Owen, R. C., Zhang, B., Ampadu, M. T., Kumar, S., Dzepina, K., Dziobak, M. P., Fialho, P., Perlinger, J. A., Hueber, J., Helmig, D., Mazzoleni, L. R. and Mazzoleni, C.: Morphology and mixing state of aged soot particles at a remote marine free troposphere site: implications for optical properties, Geophys. Res. Lett., 42(4), 1243–1250, doi:10.1002/2014GL062404, 2015.

Chow, J. C., Watson, J. G., Lowenthal, D. H., Antony Chen, L. W. and Motallebi, N.: $PM_{2.5}$ source profiles for black and organic carbon emission inventories, Atmos. Environ., 45(31), 5407–5414, doi:10.1016/j.atmosenv.2011.07.011, 2011.

Cong, Z., Kang, S., Gao, S., Zhang, Y., Li, Q. and Kawamura, K.: Historical trends of atmospheric black carbon on Tibetan Plateau as reconstructed from a 150-year lake sediment record, Environ. Sci. Technol., 47(6), 2579–2586, doi:10.1021/es3048202, 2013.

Dhammapala, R., Claiborn, C., Simpson, C. and Jimenez, J.: Emission factors from wheat and Kentucky bluegrass stubble burning: comparison of field and simulated burn experiments, Atmos. Environ., 41(7), 1512–1520, doi:10.1016/j.atmosenv.2006.10.008, 2007.

Ding, A. J., Huang, X., Nie, W., Sun, J. N., Kerminen, V. M., Petäjä, T., Su, H., Cheng, Y. F., Yang, X.-Q., Wang, M. H., Chi, X. G., Wang, J. P., Virkkula, A., Guo, W. D., Yuan, J., Wang, S. Y., Zhang, R. J., Wu, Y. F., Song, Y., Zhu, T., Zilitinkevich, S., Kulmala, M. and Fu, C. B.: Enhanced haze pollution by black carbon in megacities in China, Geophys. Res. Lett., 43(6), 2873–2879, doi:10.1002/2016GL067745, 2016.

Guo, S., Hu, M., Zamora, M. L., Peng, J., Shang, D., Zheng, J., Du, Z., Wu, Z., Shao, M., Zeng, L., Molina, M. J. and Zhang, R.: Elucidating severe urban haze formation in China, Proceedings of the National Academy of Sciences, 111(49), 17373–17378, doi:10.1073/pnas.1419604111, 2014.

Guo, Q., Hu, M., Guo, S., Wu, Z., Peng, J. and Wu, Y.: The variability in the relationship between black carbon and carbon monoxide over the eastern coast of China: BC aging during transport, Atmos. Chem. Phys., 17(17), 10395–10403, doi:10.5194/acp-17-10395-2017, 2017.

Han, S., Kondo, Y., Oshima, N., Takegawa, N., Miyazaki, Y., Hu, M., Lin, P., Deng, Z., Zhao, Y., Sugimoto, N. and Wu, Y.: Temporal variations of elemental carbon in Beijing, J. Geophys. Res., 114(D23), doi:10.1029/2009JD012027, 2009.

Hansen, J., Sato, M., Ruedy, R., Lacis, A. and Oinas, V.: Global warming in the twenty-first century: an alternative scenario, Proc. Natl. Acad. Sci., 97(18), 9875–9880, doi:10.1073/pnas.170278997, 2000.

Healy, R. M., Sofowote, U., Su, Y., Debosz, J., Noble, M., Jeong, C. H., Wang, J. M., Hilker, N., Evans, G. J., Doerksen, G., Jones, K. and Munoz, A.: Ambient measurements and source apportionment of fossil fuel and biomass burning black carbon in Ontario, Atmos. Environ., 161, 34–47, doi:10.1016/j.atmosenv.2017.04.034, 2017.

~~Henry, R., Norris, G. A., Vedantham, R. and Turner, J. R.: Source region identification using kernel smoothing, Environ. Sci. Technol., 43(11), 4090–4097, doi:10.1021/es8011723, 2009.~~

Huang, L., Gong, S. L., Sharma, S., Lavoué, D. and Jia, C. Q.: A trajectory analysis of atmospheric transport of black carbon aerosols to Canadian high Arctic in winter and spring (1990–2005), Atmos. Chem. Phys., 10(11), 5065–5073, doi:10.5194/acp-10-5065-2010, 2010.

Huang, X.-F., Sun, T.-L., Zeng, L.-W., Yu, G.-H. and Luan, S.-J.: Black carbon aerosol characterization in a coastal city in South China using a single particle soot photometer, Atmos. Environ., 51, 21–28, doi:10.1016/j.atmosenv.2012.01.056, 2012.

Huang, R. J., Zhang, Y., Bozzetti, C., Ho, K. F., Cao, J. J., Han, Y., Daellenbach, K. R., Slowik, J. G., Platt, S. M., Canonaco, F., Zotter, P., Wolf, R., Pieber, S. M., Bruns, E. A., Crippa, M., Ciarelli, G., Piazzalunga, A., Schwikowski, M., Abbaszade, G., Schnelle-Kreis, J., Zimmermann, R., An, Z., Szidat, S., Baltensperger, U., Haddad, I. E. and Prévôt, A. S. H.: High secondary aerosol contribution to particulate pollution during haze events in China, Nature, 514(7521), 218–222, doi:10.1038/nature13774, 2014.

Hyvärinen, A. P., Kolmonen, P., Kerminen, V. M., Virkkula, A., Leskinen, A., Komppula, M., Hatakka, J., Burkhart, J., Stohl, A., Aalto, P., Kulmala, M., Lehtinen, K. E. J., Viisanen, Y. and Lihavainen, H.: Aerosol black carbon at five background measurement sites over Finland, a gateway to the Arctic, Atmos. Environ., 45(24), 4042–4050, doi:10.1016/j.atmosenv.2011.04.026, 2011.

Jacobson, M. Z.: A physically-based treatment of elemental carbon optics: implications for global direct forcing of aerosols, Geophys. Res. Lett., 27(2), 217–220, doi:10.1029/1999GL010968, 2000.

Jansen, K. L., Larson, T. V., Koenig, J. Q., Mar, T. F., Fields, C., Stewart, J. and Lippmann, M.: Associations between health effects and particulate matter and black carbon in subjects with respiratory disease, Environ. Health Perspect., 113(12), 1741–1746, doi:10.1289/ehp.8153, 2005.

Ji, D., Li, L., Pang, B., Xue, P., Wang, L., Wu, Y., Zhang, H. and Wang, Y.: Characterization of black carbon in an urban-rural fringe area of Beijing, Environ. Pollut., 223, 524–534, doi:10.1016/j.envpol.2017.01.055, 2017.

Ji, D., Yan, Y., Wang, Z., He, J., Liu, B., Sun, Y., Gao, M., Li, Y., Cao, W., Cui, Y., Hu, B., Xin, J., Wang, L., Liu, Z., Tang, G. and Wang, Y.: Two-year continuous measurements of carbonaceous aerosols in urban Beijing, China: temporal variations, characteristics and source analyses, Chemosphere, 200, 191–200, doi:10.1016/j.chemosphere.2018.02.067, 2018.

Kalogridis, A. C., Vratolis, S., Liakakou, E., Gerasopoulos, E., Mihalopoulos, N. and Eleftheriadis, K.: Assessment of wood burning versus fossil fuel contribution to wintertime black carbon and carbon monoxide concentrations in Athens, Greece, Atmos. Chem. Phys. Discuss., 1–20, doi:10.5194/acp-2017-854, 2017.

Kondo, Y., Komazaki, Y., Miyazaki, Y., Moteki, N., Takegawa, N., Kodama, D., Deguchi, S., Nogami, M., Fukuda, M., Miyakawa, T., Morino, Y., Koike, M., Sakurai, H. and Ehara, K.: Temporal variations of elemental carbon in Tokyo, J. Geophys. Res., 111(D12), doi:10.1029/2005JD006257, 2006.

Kong, S., Yan, Q., Zheng, H., Liu, H., Wang, W., Zheng, S., Yang, G., Zheng, M., Wu, J., Qi, S., Shen, G., Tang, L., Yin, Y., Zhao, T., Yu, H., Liu, D., Zhao, D., Zhang, T., Ruan, J. and Huang, M.: Substantial reductions in ambient PAHs pollution and lives saved as a co-benefit of effective long-term $PM_{2.5}$ pollution controls, Environ. Int., 114, 266–279, doi:10.1016/j.envint.2018.03.002, 2018.

Lin, C. Q., Liu, G., Lau, A. K. H., Li, Y., Li, C. C., Fung, J. C. H. and Lao, X. Q.: High-resolution satellite remote sensing of provincial $PM_{2.5}$ trends in China from 2001 to 2015, Atmos. Environ., 180, 110–116, doi:10.1016/j.atmosenv.2018.02.045, 2018.

Liu, Y., Yan, C. and Zheng, M.: Source apportionment of black carbon during winter in Beijing, Sci. Total Environ., 618, 531–541, doi:10.1016/j.scitotenv.2017.11.053, 2018a

Liu, C., Chung, C. E., Yin, Y. and Schnaiter, M.: The absorption Ångström exponent of black carbon: from numerical aspects, Atmos. Chem. Phys., 18(9), 6259–6273, doi:10.5194/acp-18-6259-2018, 2018ba.

~~Liu, Y., Yan, C. and Zheng, M.: Source apportionment of black carbon during winter in Beijing, Sci. Total Environ., 618, 531–541, doi:10.1016/j.scitotenv.2017.11.053, 2018b.~~

Liu, D., Whitehead, J., Alfarra, M. R., Reyes-Villegas, E., Spracklen, D. V., Reddington, C. L., Kong, S., Williams, P. I., Ting, Y. C., Haslett, S., Taylor, J. W., Flynn, M. J., Morgan, W. T., McFiggans, G., Coe, H. and Allan, J. D.: Black-carbon absorption enhancement in the atmosphere determined by particle mixing state, Nat. Geosci., 10(3), 184–188, doi:10.1038/ngeo2901, 2017a.

Liu, D., Li, J., Cheng, Z., Zhong, G., Zhu, S., Ding, P., Shen, C., Tian, C., Chen, Y., Zhi, G. and Zhang, G.: Sources of non-fossil-fuel emissions in carbonaceous aerosols during early winter in Chinese cities, Atmos. Chem. Phys., 17(18), 11491–11502, doi:10.5194/acp-17-11491-2017, 2017b.

Liu, Q., Ma, T., Olson, M. R., Liu, Y., Zhang, T., Wu, Y. and Schauer, J. J.: Temporal variations of black carbon during haze and non-haze days in Beijing, Sci. Rep., 6(1), doi:10.1038/srep33331, 2016.

McMeeking, G. R., Hamburger, T., Liu, D., Flynn, M., Morgan, W. T., Northway, M., Highwood, E. J., Krejci, R., Allan, J. D., Minikin, A. and Coe, H.: Black carbon measurements in the boundary layer over western and northern Europe, Atmos. Chem. Phys., 10(19), 9393–9414, doi:10.5194/acp-10-9393-2010, 2010.

Moffet, R. C. and Prather, K. A.: In-situ measurements of the mixing state and optical properties of soot with implications for radiative forcing estimates, Proc. Natl. Acad. Sci., 106(29), 11872–11877, doi:10.1073/pnas.0900040106, 2009.

Mouteva Gergana O., Randerson James T., Fahrni Simon M., Bush Susan E., Ehleringer James R., Xu Xiaomei, Santos Guaciara M., Kuprov Roman, Schichtel Bret A. and Czimczik Claudia I.: Using radiocarbon to constrain black and organic carbon aerosol sources in Salt Lake City, J. Geophys. Res. Atmos., 122(18), 9843–9857, doi:10.1002/2017JD026519, 2017.

Niu, H., Kang, S., Wang, H., Zhang, R., Lu, X., Qian, Y., Paudyal, R., Wang, S., Shi, X. and Yan, X.: Seasonal variation and light absorption property of carbonaceous aerosol in a typical glacier region of the southeastern Tibetan Plateau, Atmos. Chem. Phys., 18(9), 6441–6460, doi:10.5194/acp-18-6441-2018, 2018.

Olson, M. R., Victoria Garcia, M., Robinson, M. A., Van Rooy, P., Dietenberger, M. A., Bergin, M. and Schauer, J. J.: Investigation of black and brown carbon multiple-wavelength-dependent light absorption from biomass and fossil fuel combustion source emissions, J. Geophys. Res. Atmos., 120(13), 6682–6697, doi:10.1002/2014JD022970, 2015.

Pan, X. L., Kanaya, Y., Wang, Z. F., Liu, Y., Pochanart, P., Akimoto, H., Sun, Y. L., Dong, H. B., Li, J., Irie, H. and Takigawa, M.: Correlation of black carbon aerosol and carbon monoxide in the high-altitude environment of Mt. Huang in eastern China, Atmos. Chem. Phys., 11(18), 9735–9747, doi:10.5194/acp-11-9735-2011, 2011.

Park, R. J., Jacob, D. J., Palmer, P. I , Clarke, A. D., Weber, R. J., Zondlo, M. A., Eisele, F. L., Bandy, A. R., Thornton, D. C., Sachse, G. W., and Bond, T. C.: Export efficiency of black carbon aerosol in continental outflow: global implications, J. Geophys. Res., 110(D11), doi:10.1029/2004JD005432, 2005.

Peng, J., Hu, M., Guo, S., Du, Z., Zheng, J., Shang, D., Levy Zamora, M., Zeng, L., Shao, M., Wu, Y. S., Zheng, J., Wang, Y., Glen, C. R., Collins, D. R., Molina, M. J. and Zhang, R.: Markedly enhanced absorption and direct radiative forcing of black carbon under polluted urban environments, Proc. Natl. Acad. Sci., 113(16), 4266–4271, doi:10.1073/pnas.1602310113, 2016.

Petit, J. E., Favez, O., Sciare, J., Crenn, V., Sarda-Estève, R., Bonnaire, N., Močnik, G., Dupont, J. C., Haeffelin, M. and Leoz-Garziandia, E.: Two years of near real-time chemical composition of submicron aerosols in the region of Paris using an Aerosol Chemical Speciation Monitor (ACSM) and a multi-wavelength Aethalometer, Atmos. Chem. Phys., 15(6), 2985–3005, doi:10.5194/acp-15-2985-2015, 2015.

Petit, J. E., Favez, O., Albinet, A. and Canonaco, F.: A user-friendly tool for comprehensive evaluation of the geographical origins of atmospheric pollution: wind and trajectory analyses, Environ. Model. Softw., 88, 183–187, doi:10.1016/j.envsoft.2016.11.022, 2017a.

Petit, J. E., Amodeo, T., Meleux, F., Bessagnet, B., Menut, L., Grenier, D., Pellan, Y., Ockler, A., Rocq, B., Gros, V., Sciare, J. and Favez, O.: Characterising an intense PM pollution episode in March 2015 in France from multi-site approach and near real time data: climatology, variabilities, geographical origins and model evaluation, Atmos. Environ., 155, 68–84, doi:10.1016/j.atmosenv.2017.02.012, 2017b.

Qi, L., Li, Q., Henze, D. K., Tseng, H. L. and He, C.: Sources of springtime surface black carbon in the Arctic: an adjoint analysis for April 2008, Atmos. Chem. Phys., 17(15), 9697–9716, doi:10.5194/acp-17-9697-2017, 2017.

Qin, Y. and Xie, S. D.: Spatial and temporal variation of anthropogenic black carbon emissions in China for the period 1980–2009, Atmos. Chem. Phys., 12(11), 4825–4841, doi:10.5194/acp-12-4825-2012, 2012.

Qiu, X., Duan, L., Chai, F., Wang, S., Yu, Q. and Wang, S.: Deriving high-resolution emission inventory of open biomass burning in China based on satellite observations, Environ. Sci. Technol., 50(21), 11779–11786, doi:10.1021/acs.est.6b02705, 2016.

Rajesh, T. A. and Ramachandran, S.: Black carbon aerosol mass concentration, absorption and single scattering albedo from single and dual spot aethalometers: radiative implications, J. Aerosol Sci., 119, 77–90, doi:10.1016/j.jaerosci.2018.02.001, 2018.

Riemer, N., Vogel, H. and Vogel, B.: Soot aging time scales in polluted regions during day and night, Atmos. Chem. Phys., 4(7), 1885–1893, doi:10.5194/acp-4-1885-2004, 2004.

Salma, I., Németh, Z., Weidinger, T., Maenhaut, W., Claeys, M., Molnár, M., Major, I., Ajtai, T., Utry, N. and Bozóki, Z.: Source apportionment of carbonaceous chemical species to fossil fuel combustion, biomass burning and biogenic emissions by a coupled radiocarbon–levoglucosan marker method, Atmos. Chem. Phys., 17(22), 13767–13781, doi:10.5194/acp-17-13767-2017, 2017.

Sandradewi, J., Prévôt, A. S. H., Szidat, S., Perron, N., Alfarra, M. R., Lanz, V. A., Weingartner, E. and Baltensperger, U.: Using aerosol light absorption measurements for the quantitative determination of wood Burning and traffic emission contributions to particulate matter, Environ. Sci. Technol., 42(9), 3316–3323, doi:10.1021/es702253m, 2008.

Schnaiter, M.: Absorption amplification of black carbon internally mixed with secondary organic aerosol, ~~Journal~~ J.~~of Geophysical~~ Geophys. ~~Research~~Res., 110(D19), doi:10.1029/2005JD006046, 2005.

Singh, S., Fiddler, M. N. and Bililign, S.: Measurement of size-dependent single scattering albedo of fresh biomass burning aerosols using the extinction-minus-scattering technique with a combination of cavity ring-down spectroscopy and nephelometry, Atmos. Chem. and Phys., 16(21), 13491–13507, doi:10.5194/acp-16-13491-2016, 2016.

Streets, D. G., Bond, T. C., Carmichael, G. R., Fernandes, S. D., Fu, Q., He, D., Klimont, Z., Nelson, S. M., Tsai, N. Y., Wang, M. Q., Woo, J. H. and Yarber, K. F.: An inventory of gaseous and primary aerosol emissions in Asia in the year 200, J. Geophys. Res. Atmos., 108(D21), doi:10.1029/2002JD003093, 2003.

Sun, J., Zhi, G., Hitzenberger, R., Chen, Y., Tian, C., Zhang, Y., Feng, Y., Cheng, M., Zhang, Y., Cai, J., Chen, F., Qiu, Y., Jiang, Z., Li, J., Zhang, G. and Mo, Y.: Emission factors and light absorption properties of brown carbon from household coal combustion in China, Atmos. Chem. Phys., 17(7), 4769–4780, doi:10.5194/acp-17-4769-2017, 2017.

Tao, J., Zhang, L., Cao, J. and Zhang, R.: A review of current knowledge concerning $PM_{2.5}$: chemical composition, aerosol optical properties and their relationships across China, Atmos. Chem. Phys., 17(15), 9485–9518, doi:10.5194/acp-17-9485-2017, 2017.

Verma, R. L., Sahu, L. K., Kondo, Y., Takegawa, N., Han, S., Jung, J. S., Kim, Y. J., Fan, S., Sugimoto, N., Shammaa, M. H., Zhang, Y. H. and Zhao, Y.: Temporal variations of black carbon in Guangzhou, China, in summer 2006, Atmos. Chem. Phys., 10(14), 6471–6485, doi:10.5194/acp-10-6471-2010, 2010.

Wang, Y., Wang, X., Kondo, Y., Kajino, M., Munger, J. W. and Hao, J.: Black carbon and its correlation with trace gases at a rural site in Beijing: top-down constraints from ambient measurements on bottom-up emissions, J. Geophys. Res. Atmos., 116(D24), doi:10.1029/2011JD016575, 2011.

~~Wang, H., He, Q., Chen, Y. and Kang, Y.: Characterization of black carbon concentrations of haze with different intensities in Shanghai by a three-year field measurement, Atmos. Environ., 99, 536–545, doi:10.1016/j.atmosenv.2014.10.025, 2014a.~~

Wang, R., Tao, S., Balkanski, Y., Ciais, P., Boucher, O., Liu, J., Piao, S., Shen, H., Vuolo, M. R., Valari, M., Chen, H., Chen, Y., Cozic, A., Huang, Y., Li, B., Li, W., Shen, G., Wang, B. and Zhang, Y.: Exposure to ambient black carbon derived from a unique inventory and high-resolution model, Proc. Natl. Acad. Sci., 111(7), 2459–2463, doi:10.1073/pnas.1318763111, 2014a~~b~~.

Wang, Q., Huang, R.-J., Cao, J., Han, Y., Wang, G., Li, G., Wang, Y., Dai, W., Zhang, R. and Zhou, Y.: Mixing state of black carbon aerosol in a heavily polluted urban area of China: implications for light absorption enhancement, Aerosol. Sci. and Tech., 48(7), 689–697, doi:10.1080/02786826.2014.917758, 2014b.

Wang, H., He, Q., Chen, Y. and Kang, Y.: Characterization of black carbon concentrations of haze with different intensities in Shanghai by a three-year field measurement, Atmos. Environ., 99, 536–545, doi:10.1016/j.atmosenv.2014.10.025, 2014c

Wang, J., Virkkula, A., Gao, Y., Lee, S., Shen, Y., Chi, X., Nie, W., Liu, Q., Xu, Z., Huang, X., Wang, T., Cui, L. and Ding, A.: Observations of aerosol optical properties at a coastal site in Hong Kong, South China, Atmos. Chem. Phys., 17(4), 2653–2671, doi:10.5194/acp-17-2653-2017, 2017a.

Wang, Y., de Foy, B., Schauer, J. J., Olson, M. R., Zhang, Y., Li, Z. and Zhang, Y.: Impacts of regional transport on black carbon in Huairou, Beijing, China, Environ. Pollut., 221, 75–84, doi:10.1016/j.envpol.2016.11.006, 2017b.

Wang, Q., Cao, J., Han, Y., Tian, J., Zhu, C., Zhang, Y., Zhang, N., Shen, Z., Ni, H., Zhao, S. and Wu, J.: Sources and physicochemical characteristics of black carbon aerosol from the southeastern Tibetan Plateau: internal mixing enhances light absorption, Atmos. Chem. Phys., 18(7), 4639–4656, doi:10.5194/acp-18-4639-2018, 2018a.

Wang, Z., Huang, X. and Ding, A.: Dome effect of black carbon and its key influencing factors: a one-dimensional modelling study, Atmos. Chem. Phys., 18(4), 2821–2834, doi:10.5194/acp-18-2821-2018, 2018b.

Wang, Y., Ma, P.-L., Peng, J., Zhang, R., Jiang, J. H., Easter, R. C. and Yung, Y. L.: Constraining aging processes of black carbon in the community atmosphere model using environmental chamber measurements, J. Adv. in Model Earth Sys., 10(10), 2514–2526, doi:10.1029/2018MS001387, 2018c.

Weingartner, E., Saathoff, H., Schnaiter, M., Streit, N., Bitnar, B. and Baltensperger, U.: Absorption of light by soot particles: determination of the absorption coefficient by means of aethalometers, J. Aerosol Sci., 34(10), 1445–1463, doi:10.1016/S0021-8502(03)00359-8, 2003.

Weller, R., Minikin, A., Petzold, A., Wagenbach, D. and König-Langlo, G.: Characterization of long-term and seasonal variations of black carbon (BC) concentrations at Neumayer, Antarctica, Atmos. Chem. Phys, 13(3), 1579–1590, doi:10.5194/acp-13-1579-2013, 2013.

Westerdahl, D., Wang, X., Pan, X. and Zhang, K. M.: Characterization of on-road vehicle emission factors and microenvironmental air quality in Beijing, China, Atmos. Environ., 43(3), 697–705, doi:10.1016/j.atmosenv.2008.09.042, 2009.

Wu, D., Mao, J., Deng, X., Tie, X., Zhang, Y., Zeng, L., Li, F., Tan, H., Bi, X., Huang, X., Chen, J. and Deng, T.: Black carbon aerosols and their radiative properties in the Pearl River Delta region, Sci. China Ser. Earth Sci., 52(8), 1152–1163, doi:10.1007/s11430-009-0115-y, 2009.

Xu, J. W., Martin, R. V., Morrow, A., Sharma, S., Huang, L., Leaitch, W. R., Burkart, J., Schulz, H., Zanatta, M., Willis, M. D., Henze, D. K., Lee, C. J., Herber, A. B. and Abbatt, J. P. D.: Source attribution of Arctic black carbon constrained by aircraft and surface measurements, Atmos. Chem. Phys., 17(19), 11971–11989, doi:10.5194/acp-17-11971-2017, 2017.

Yang, Y., Wang, H., Smith, S. J., Ma, P. L. and Rasch, P. J.: Source attribution of black carbon and its direct radiative forcing in China, Atmos. Chem. Phys., 17(6), 4319–4336, doi:10.5194/acp-17-4319-2017, 2017.

Zhang, Q., Streets, D. G., Carmichael, G. R., He, K. B., Huo, H., Kannari, A., Klimont, Z., Park, I. S., Reddy, S., Fu, J. S., Chen, D., Duan, L., Lei, Y., Wang, L. T. and Yao, Z. L.: Asian emissions in 2006 for the NASA INTEX-B mission, Atmos. Chem. Phys., 9(14), 5131–5153, doi:10.5194/acp-9-5131-2009, 2009.

Zhang, X., Rao, R., Huang, Y., Mao, M., Berg, M. J. and Sun, W.: Black carbon aerosols in urban central China, J. Quant. Spectrosc. Radiat. Transf., 150, 3–11, doi:10.1016/j.jqsrt.2014.03.006, 2015a.

Zhang, Y. L., Huang, R. J., El Haddad, I., Ho, K. F., Cao, J. J., Han, Y., Zotter, P., Bozzetti, C., Daellenbach, K. R., Canonaco, F., Slowik, J. G., Salazar, G., Schwikowski, M., Schnelle-Kreis, J., Abbaszade, G., Zimmermann, R., Baltensperger, U., Prévôt, A. S. H. and Szidat, S.: Fossil vs. non-fossil sources of fine carbonaceous aerosols in four Chinese cities during the extreme winter haze episode of 2013, Atmos. Chem. Phys., 15(3), 1299–1312, doi:10.5194/acp-15-1299-2015, 2015b.

Zhang, K., Wang, D., Bian, Q., Duan, Y., Zhao, M., Fei, D., Xiu, G. and Fu, Q.: Tethered balloon-based particle number concentration, and size distribution vertical profiles within the lower troposphere of Shanghai, Atmos. Environ., 154, 141–150, doi:10.1016/j.atmosenv.2017.01.025, 2017.

Zhang, Y., Zhang, Q., Cheng, Y., Su, H., Li, H., Li, M., Zhang, X., Ding, A. and He, K.: Amplification of light absorption of black carbon associated with air pollution, Atmos. Chem. Phys., 1–27, doi:10.5194/acp-2017-983, 2018.

Zhao, P., Dong, F., Yang, Y., He, D., Zhao, X., Zhang, W., Yao, Q. and Liu, H.: Characteristics of carbonaceous aerosol in the region of Beijing, Tianjin, and Hebei, China, Atmos. Environ., 71, 389–398, doi:10.1016/j.atmosenv.2013.02.010, 2013.

Zheng, G. J., Duan, F. K., Su, H., Ma, Y. L., Cheng, Y., Zheng, B., Zhang, Q., Huang, T., Kimoto, T., Chang, D., Pöschl, U., Cheng, Y. F. and He, K. B.: Exploring the severe winter haze in Beijing: the impact of synoptic weather, regional transport and heterogeneous reactions, Atmos. Chem. Phys., 15(6), 2969–2983, doi:10.5194/acp-15-2969-2015, 2015.

Zheng, H., Kong, S., Xing, X., Mao, Y., Hu, T., Ding, Y., Li, G., Liu, D., Li, S. and Qi, S.: Monitoring of volatile organic compounds (VOCs) from an oil and gas station in northwest China for 1 year, Atmos. Chem. Phys., 18(7), 4567–4595, doi:10.5194/acp-18-4567-2018, 2018.

Zhu, C. S., Cao, J. J., Hu, T. F., Shen, Z. X., Tie, X. X., Huang, H., Wang, Q. Y., Huang, R. J., Zhao, Z.Z., Močnik, G. and Hansen, A. D. A.: Spectral dependence of aerosol light absorption at an urban and a remote site over the Tibetan Plateau, Sci. Total Environ., 590–591, 14–21, doi:10.1016/j.scitotenv.2017.03.057, 2017.

Zhuang, B. L., Wang, T. J., Liu, J., Li, S., Xie, M., Yang, X. Q., Fu, C. B., Sun, J. N., Yin, C. Q., Liao, J. B., Zhu, J. L. and Zhang, Y.: Continuous measurement of black carbon aerosol in urban Nanjing of Yangtze River Delta, China, Atmos. Environ., 89, 415–424, doi:10.1016/j.atmosenv.2014.02.052, 2014.

Zhuang, B. L., Wang, T. J., Liu, J., Ma, Y., Yin, C. Q., Li, S., Xie, M., Han, Y., Zhu, J. L., Yang, X. Q. and Fu, C. B.: Absorption coefficient of urban aerosol in Nanjing, west Yangtze River Delta, China, Atmos. Chem. Phys., 15(23), 13633–13646, doi:10.5194/acp-15-13633-2015, 2015.

Zhuang, B., Wang, T., Liu, J., Li, S., Xie, M., Han, Y., Chen, P., Hu, Q., Yang, X., Fu, C. and Zhu, J.: The surface aerosol optical properties in the urban area of Nanjing, west Yangtze River Delta, China, Atmos. Chem. Phys., 17(2), 1143–1160, doi:10.5194/acp-17-1143-2017, 2017.

Zotter, P., Herich, H., Gysel, M., El-Haddad, I., Zhang, Y., Močnik, G., Hüglin, C., Baltensperger, U., Szidat, S. and Prévôt, A. S. H.: Evaluation of the absorption Ångström exponents for traffic and wood burning in the Aethalometer based source apportionment using radiocarbon measurements of ambient aerosol, Atmos. Chem. Phys. Discuss., 1–29, doi:10.5194/acp-2016-621, 2016.

Table 1 Information of the observation sites, periods and instruments

Sampling site	Location	Site type	Sampling period	Instrument	Data resolution
Hong'an (HA)	114.58º E, 31.24º N	Rural	1/8 13:00~1/25 9:00, 2018	AE33	1-minute
Luohe (LH)	114.05º E, 33.57º N	Suburban	1/9 18:00~1/25 9:00, 2018	AE33	1-minute
Suixian (SX)	113.28º E, 31.88º N	Rural	1/10 09:00~1/25 8:00, 2018	AE51	1-minute
Wuhan (WH)	114.39º E, 30.53º N	Urban	1/8 15:00~1/25 8:00, 2018	AE31	5-minute
Xiangyang (XY)	112.17º E, 32.02º N	Suburban	1/10 09:00~1/25 8:00, 2018	AE51	1-minute

Table 2 Ratios of BC/CO (mean ± standard deviation) at the five sites under different air pollution situation

Sampling site	BC/CO (μg m^{-3}/ppbv)		
	Clean	Light pollution	Heavy pollution
HA	0.0048 ± 0.008	0.0057 ± 0.013	—[a]
LH	0.0058 ± 0.0024	0.0072 ± 0.0023	0.0071 ± 0.0013
SX	0.0025 ± 0.0013	0.0042 ± 0.0013	–
WH	0.0045 ± 0.0022	0.0042 ± 0.0017	–
XY	0.0048 ± 0.0020	0.0060 ± 0.0031	0.0071 ± 0.0040

[a] No heavy pollution episodes were observed

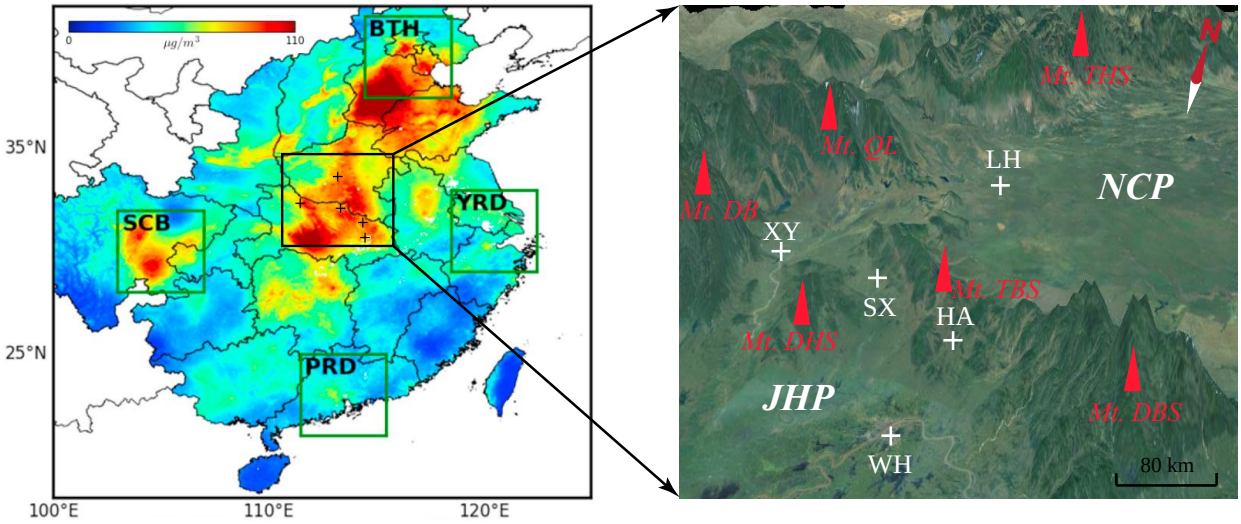
0
μg/m³
110
BTH
YRD
SCB
PRD
35°N
25°N
100°E
110°E
120°E
Mt. THS
Mt. QL
Mt. DB
LH
NCP
XY
SX
HA
Mt. TBS
Mt. DHS
JHP
Mt. DBS
WH
80 km
N

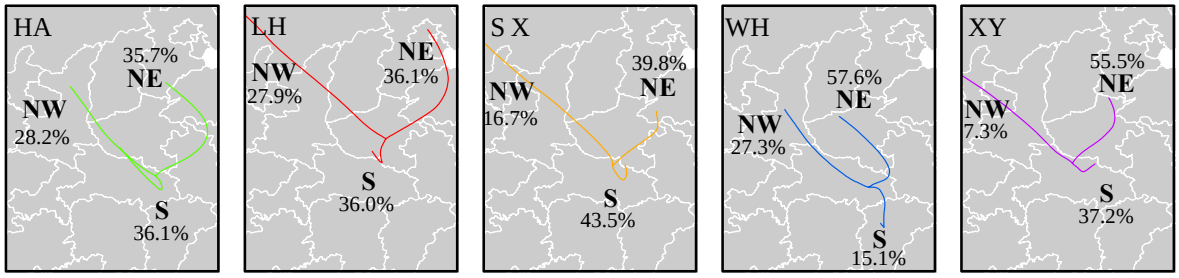
HA
35.7%
NE
NW
28.2%
S
36.1%
LH
NE
36.1%
NW
27.9%
S
36.0%
S X
39.8%
NE
NW
16.7%
S
43.5%
WH
57.6%
NE
NW
27.3%
S
15.1%
XY
55.5%
NE
NW
7.3%
S
37.2%

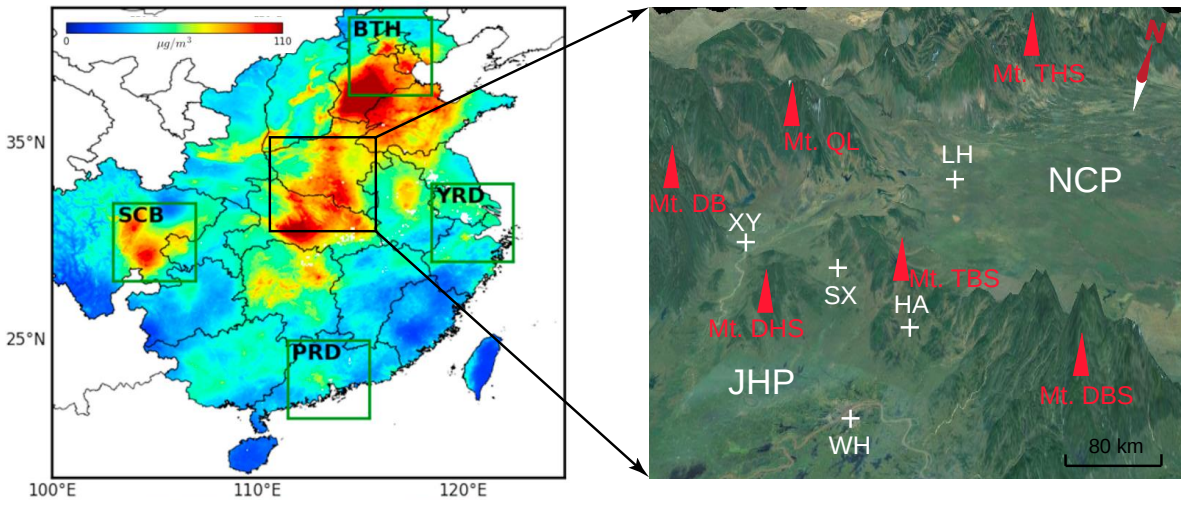
0
μg/m³
110
BTH
YRD
SCB
PRD
35°N
25°N
100°E
110°E
120°E
Mt. THS
Mt. QL
Mt. DB
LH
NCP
XY
SX
HA
Mt. TBS
Mt. DHS
JHP
Mt. DBS
WH
80 km
N

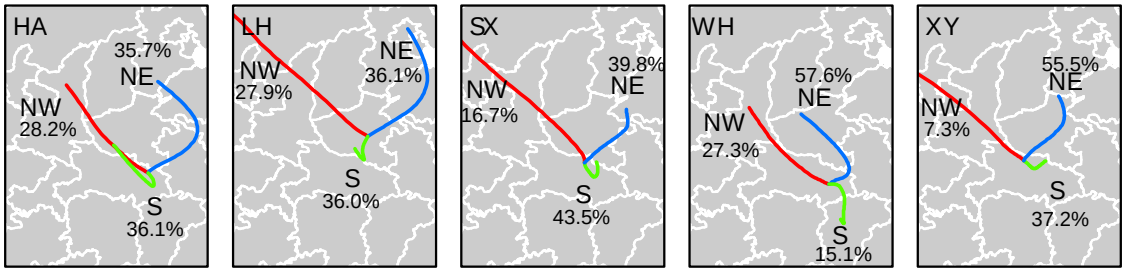
HA
35.7%
NE
NW
28.2%
S
36.1%
LH
NE
36.1%
NW
27.9%
S
36.0%
SX
39.8%
NE
NW
16.7%
S
43.5%
WH
57.6%
NE
NW
27.3%
S
15.1%
XY
55.5%
NE
NW
7.3%
S
37.2%

Figure 1 Location, terrain of the study area and clusters of backward trajectories reaching at each observation site. Up left is the spatial distribution of the 15 years average ~~of~~ $PM_{2.5}$ concentrations at a resolution of 1 km ~~in the study region~~ (Lin et al., 2018). Right up shows that the study area is surrounded by mountains and Mt. DBS and Mt. TBS blocks the North China Plain (NCP) and Jianghan Plian (JHP). Bottom shows that air masses reaching at the five sites were mainly from north directions (northwest and northeast) during the observation period.

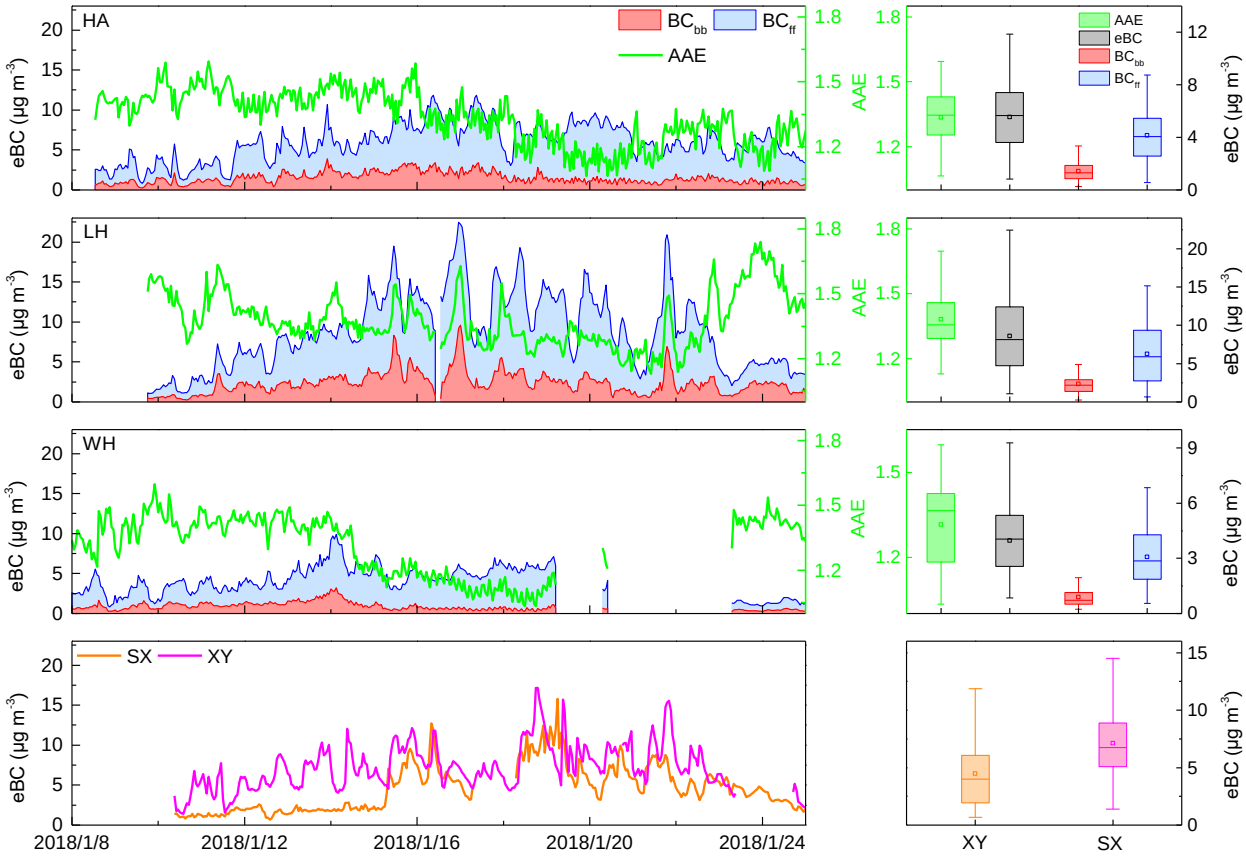

Figure 2 Time series and box plots of eBC, BC_{bb}, BC_{ff}, and absorption Ångström exponent (AAE) at the five sites during the observation period.

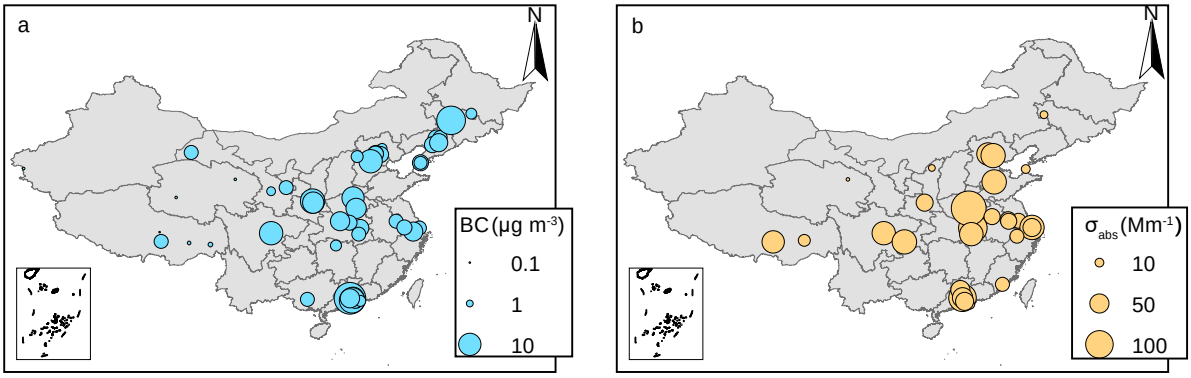

Figure 3 Spatial distribution of BC mass concentration (a) and absorption coefficients (b) in China. More details can be found in Table S1 and S2 in the supplementary materials.

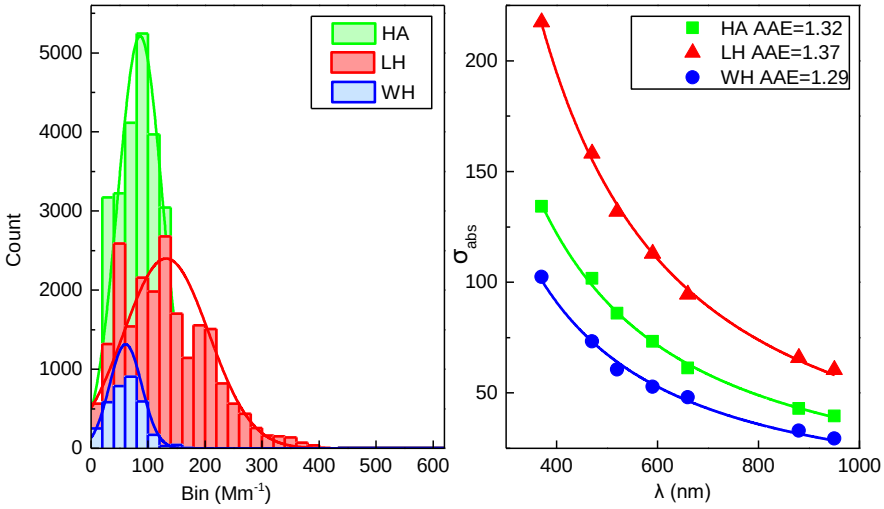

Figure ~~3~~ 4 Frequency distribution of absorption coefficients (σ~~b~~$_{abs}$) at 520 nm wavelength (left panel) and power fit of σ~~b~~$_{abs}$ at seven wavelengths (right panel) for HA, LH, and WH.

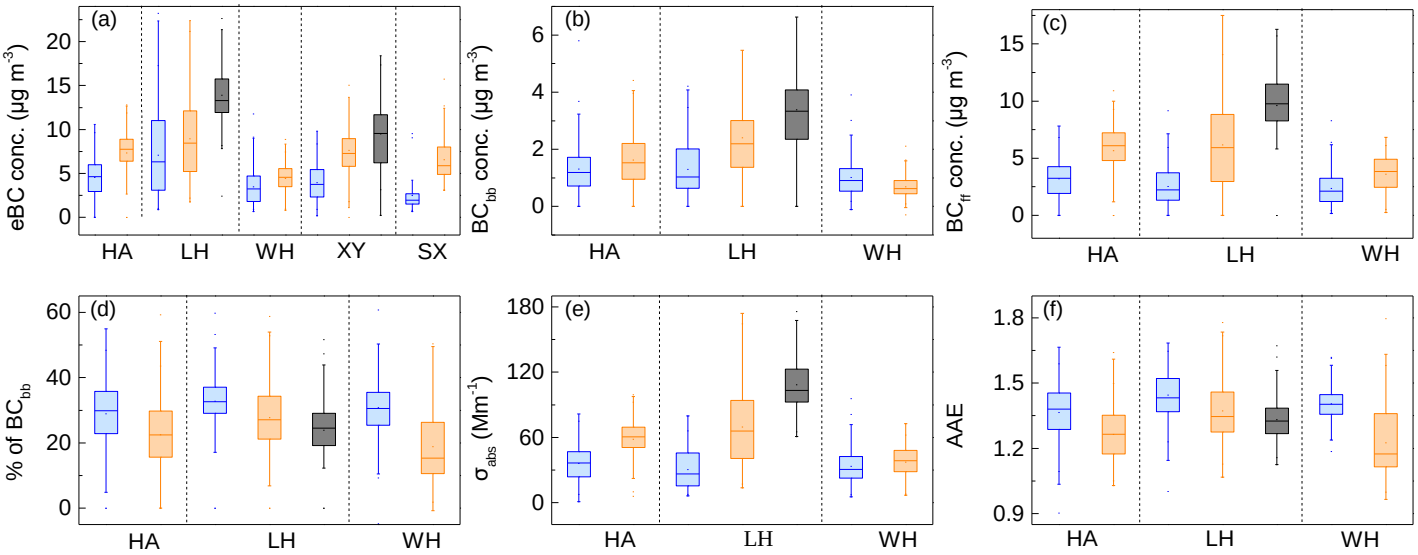

Figure 4-5 Box (25−75th percentiles) and whisker (5−95th percentiles) plots of eBC concentrations (a), BC_{bb} (b), BC_{ff} (c), percentages of BC_{bb} (d), aerosol absorption coefficients (e), and absorption Ångström exponent (AAE) under different air pollution situation. The blue, orange and black color represent the clean ($PM_{2.5}$ <75 μg m^{-3}), light pollution (75< $PM_{2.5}$ <250 μg m^{-3}) and heavy pollution conditions ($PM_{2.5}$ >250 μg m^{-3}), respectively. The data number for the different air quality could be found in the supplementary file (Table S4).

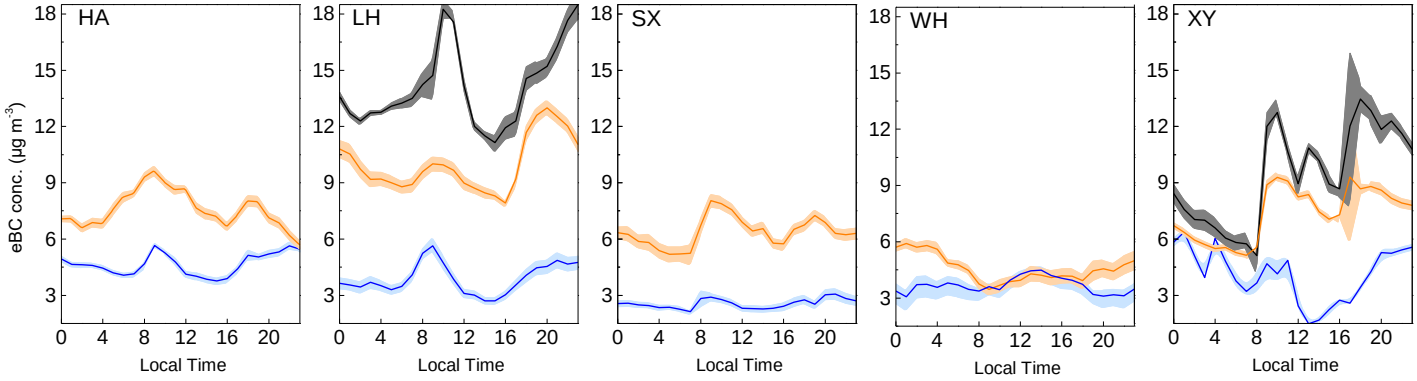

Figure ~~5~~ 6 Diurnal variations of eBC under different air pollution situations (blue: clean; orange: light polluted; dark: heavy polluted) at the five observation sites. The solid lines are the average values and the filled ribbons are 95th confidential intervals of the average value.

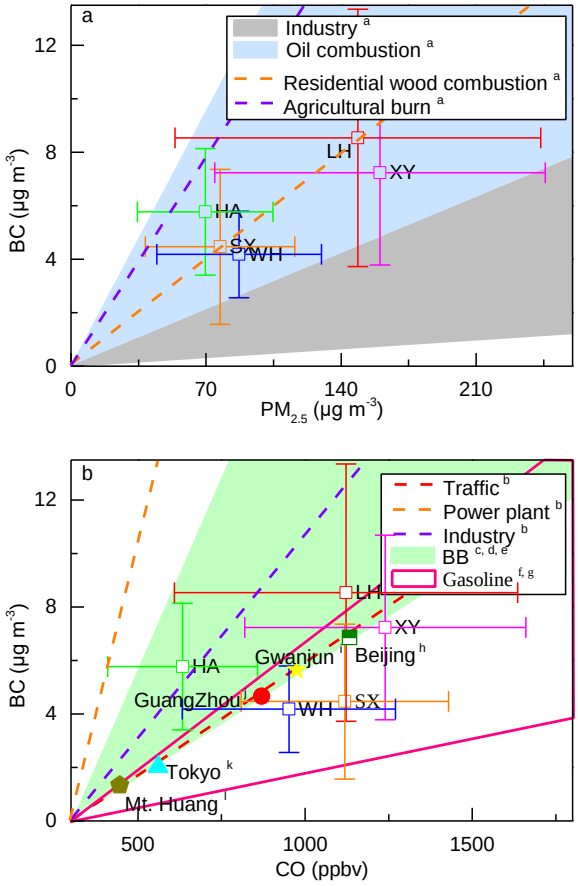

Figure ~~6~~ 7 Ratios of BC/$PM_{2.5}$ (a) and BC/CO (b) in this study and previous researches.

[a] Chow et al., (2011); [b] Zhang et al., (2009); [c] Dhammapala et al., (2007); [d] Cao et al., (2008); [e] Andreae and Merlet, (2001); [f] Streets et al., (2003); [g] Westerdahl et al., (2009); [h] Liu et al., (2018a); [i] Park et al., (2005) ; [j] Vermal et al., (2010); [k] Kondo et al., (2006); [l] Pan et al., (2011).

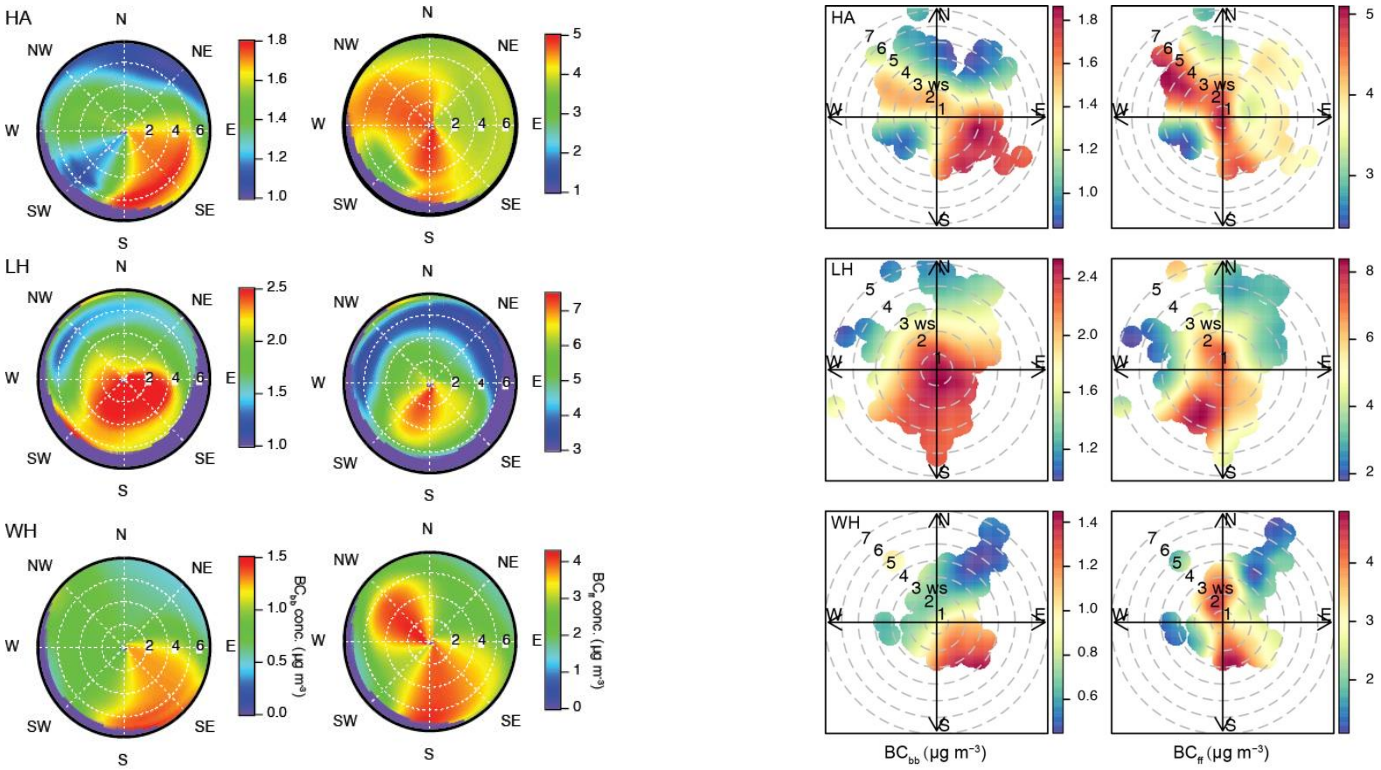

Figure ~~7~~ 8 ~~NWR~~ Conditional bivariate probability function (CBPF) plots of BC_{bb} (left panel) and BC_{ff} (right panel) at HA, LH and WH.

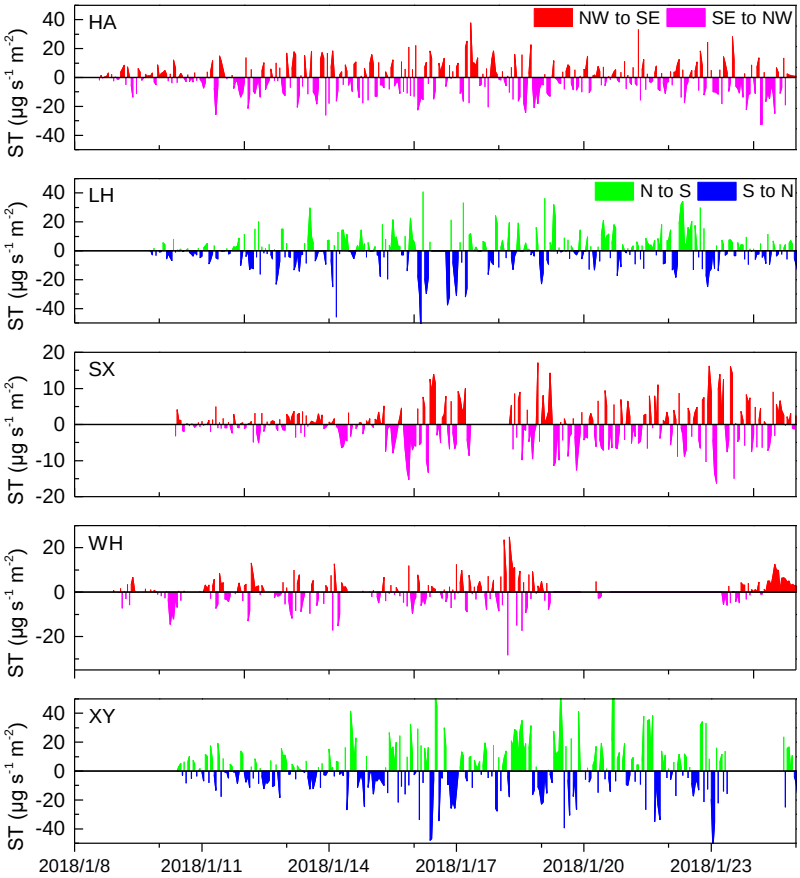

Figure ~~8~~ 9 Time series of surface transport intensity for BC at the five observation sites. Positive values for HA and LH indicated the transport direction was from north to south and negative values indicated the transport direction was from south to north. Positive values for SX, WH and XY indicated the transport directions were from northwest to southeast and negative values indicated the transport directions were from southeast to northwest.

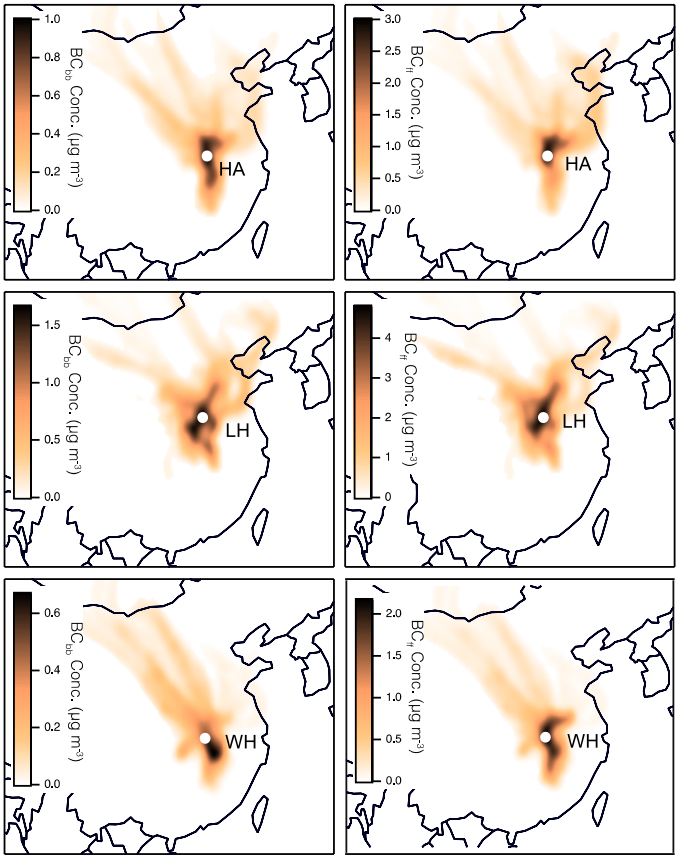

Figure 9 10 Concentration-weighted trajectory (CWT) plots of BC_{bb} (left panel) and BC_{ff} (right panel) at HA, LH and WH during the whole observation site. The white dote represents the observation site.

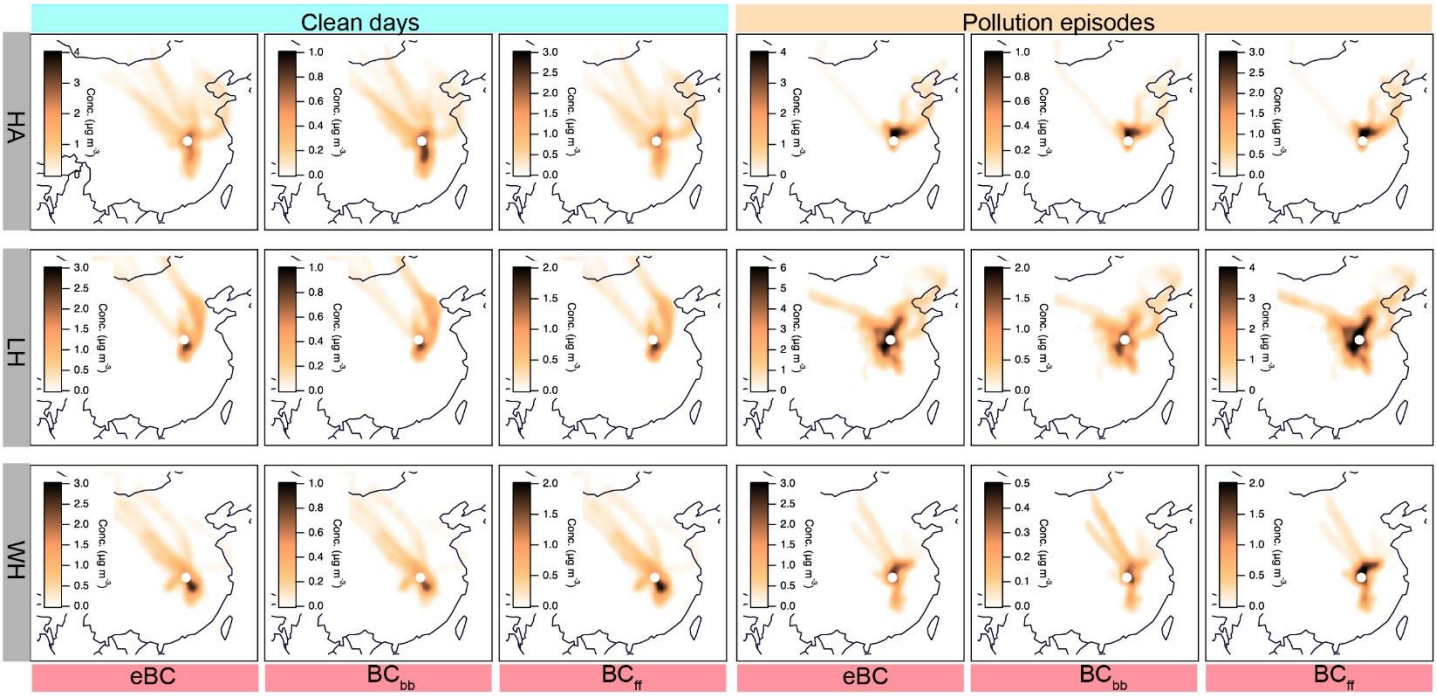

Figure ~~10~~ 11 Concentration-weighted trajectory (CWT) plots of eBC, BC_{bb} and BC_{ff} during clean and pollution episodes at HA, LH and WH. The white dot represents the observation site.

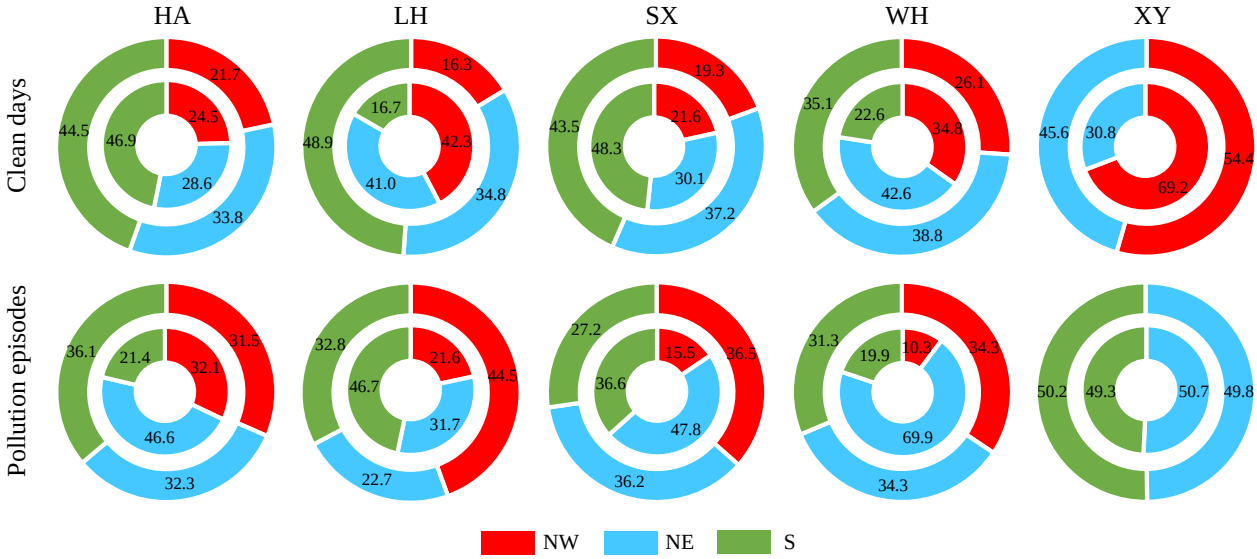

Figure 1~~2~~1 Cluster results of air masses reaching at five sites (inner pie plots) and the eBC percentage contributions from different clusters (extern pie plot) during the clean days (up panel) and pollution episodes (bottom panel). NW, NE and S mean the northwest, northeast and south direction clusters as shown in Figure 1.

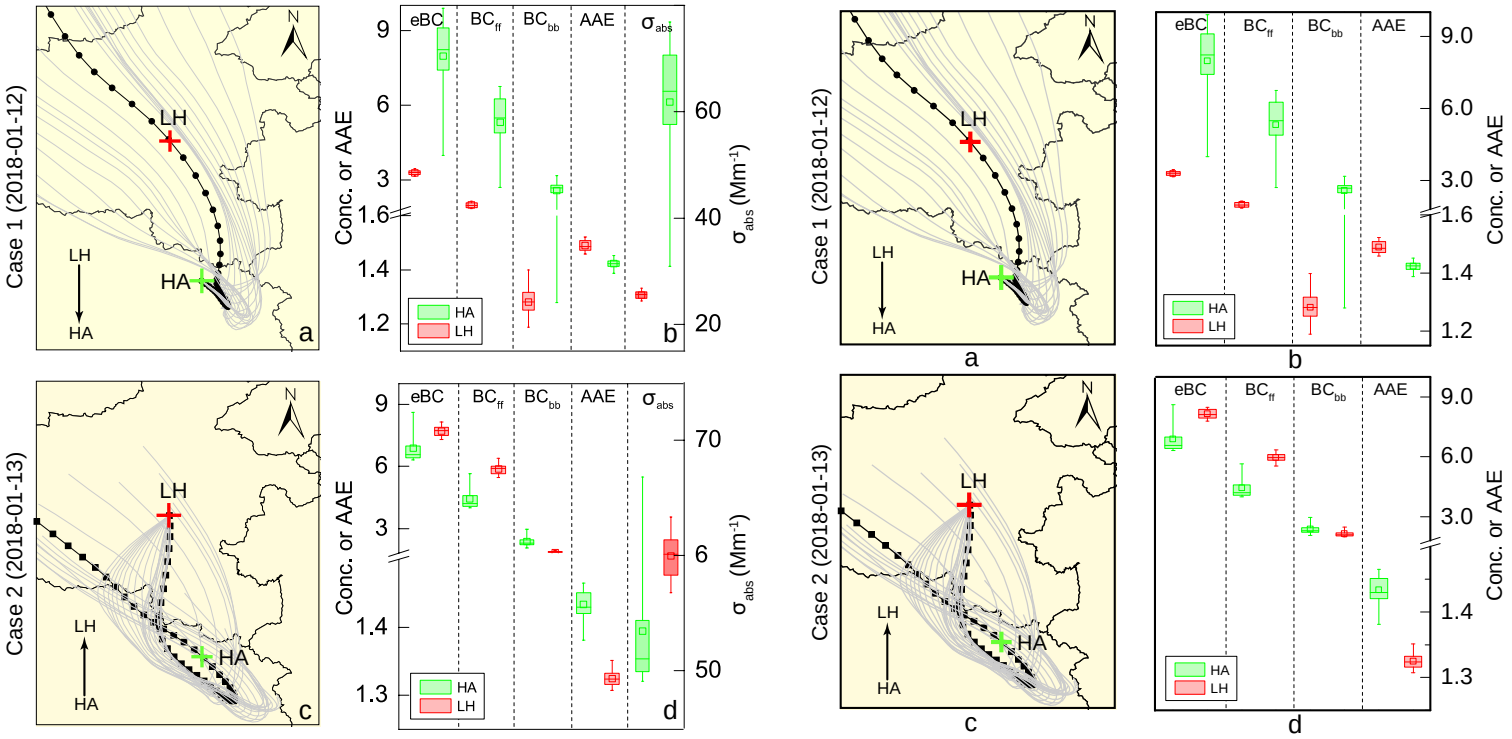

Figure 1~~3~~2 Case studies~~y~~ of BC variation during the transportation from upwind to downwind direction. a (case 1): Hourly backward trajectories (grey line) reaching at HA on 2018-1-12 and the trajectory at 13:00 (GMT~~UTC~~) (black line) was found passing through LH about 28 hours ago. c (case 2): Trajectory reaching at LH on 2018-1-13 07:00 (GMT~~UCT~~) (black line) was found passing through HA about 31 hours ago. Box (25-75th percentiles) and whisker (5-95th percentiles) plots of eBC, BC$_{ff}$, BC$_{bb}$ σ$_{abs}$, and AAE variations during the transport from LH to HA (b) and from HA to LH (d).